Visualizing Vitreous Using Quantum Dots as Imaging Agents

Satoru Yamamoto, Noriyoshi Manabe, Kouki Fujioka, Akiyoshi Hoshino, and Kenji Yamamoto*

***Abstract*—Vitreous is transparent tissue located between the lens and the retina of the eye, thus, difficult to look at by even ophthalmological microscope. But vitreous is connected with some sight-threatening eye diseases, for example, retinal detachment, macular hole, epi-retinal membrane, and so forth. Quantum dots (QDs) have been applied to a wide range of biological studies by taking advantage of their fluorescence properties. We established a novel technique of aqueous colloidal QD (ACQD) as a vitreous lesion detector. When compared with some conventional dyes used for clinical situation, i.e. fluorescein, indocyanine green, and triamcinolone acetonide, ACQD exerted a higher performance to detect a Weiss Ring. Furthermore ACQD is also effective to perform vitrectomy, an eye surgery to cut and eliminate vitreous. Some functional structures in vitreous are detected clearly when ACQD was injected into an enucleated porcine eye. We demonstrated that ACQD enabled any ophthalmic surgeon to perform vitrectomy reliably, easily, and more safely. Taken together, the ACQD-oriented vitreous staining system will promote ophthalmological science, and it will raise the cure rate of eye diseases.**

***Index Terms*—Aqueous colloidal quantum dot, vitrectomy, vitreous imaging reagents.**

I. Introduction

ALTHOUGH IT IS very important to understand the general structure and substructure of the eye [1], the lack of adequate methods to image transparent vitreous makes it very difficult to fully understand vitreous normal structure, function, and how these change during aging and disease [2], [3], because the vitreous is jellylike tissue that is filled with transparent collagen and hyaluronate. Thus, it is required to develop a new vitreous visualizing method for ophthalmologists to observe the pathology of vitreous [4]–[8]. Here we demonstrate that a novel visualizing tool with aqueous colloidal quantum dots (ACQDs) enables us to image and observe the transparent vitreous lesion clearly.[1]

It has been shown recently that many eye diseases are connected with pathologic and/or physiological changes of the vitreous. Liquefaction of vitreous through aging may be involved in retinal tear which may lead to retinal detachment, and eventually to lack of light perception. The epiretinal membrane is thought to be connected with posterior vitreous denature after liquefaction. In addition, it caused some complicated diseases such as proliferative vitreoretinopathy, macular hole, retinopathy of prematurity, and proliferative diabetic vitreoretinopathy. As for vitreous around the posterior pole of the eye, optical coherence tomography (OCT) was invented (particularly ultrahigh-resolution OCT [9]) and solved the question of macular hole formation [10], [11]. But there is no adequate method to observe transparent vitreous in daily clinical situations. In addition, it is difficult to observe the vitreous in the case of vitreous surgery (called vitrectomy). As a result, the inability to image vitreous adequately may induce unavoidable errors in the operation such as damaged retina.

Several organic dyes including fluorescein and indocyanine green have been used as imaging agents for retinal and choroidal vessels [12], but they have difficulties for diagnosis for vitreous cavity. A turbid corticosteroid, triamcinolone acetonide (TA), is also used as an imaging reagent in some special cases; improvement of diabetic macular edema or for vitrectomy, but some side effects have been reported such as the elevation of intraocular pressure, acceleration of cataract, and endophthalmitis [13]–[15]. Therefore, it is important to develop new vitreous visualizing materials and a method not only for ophthalmologists to observe the pathology of vitreous but also to treat vitreous-related diseases.

II. Materials and Methods

A. Materials

Some porcine eyes (approximately 6 months old) were purchased from Tokyo Metropolitan Slaughterhouse (Tokyo, Japan) as a virtual human eye to perform vitrectomy training for ophthalmological residents.

Some aged porcine eyes (approximately 8 years old) were provided from Tokushima A. F. F. Technology Support Center (Tokushima, Japan) as aged vitreous lesion models.

B. Synthesis and Purification of ACQDs

ACQDs were synthesized by replacing QD-TOPO with the aqueous dipeptide (1-[(2S)-3-mercapto-2-methylpropionyl]-L-

Manuscript received August 28, 2006; revised December 6, 2006. This work was supported in part by the Ministry of Health, Labor and Welfare of Japan under Medical Techniques Promotion Research Grant H14-nano-004 (K. Yamamoto), and in part by a bioimaging grant from Japan Foundation of Cardiovascular Research (A. Hoshino).

S. Yamamoto is with the Department of Ophthalmology, Yokohama Sakae Kyousai Hospital, Yokohama, Japan.

N. Manabe and K. Fujioka are with the Research Institute, International Medical Center of Japan, Shinjuku-ku, Tokyo 162-8655 Japan.

A. Hoshino is with the Research Institute, International Medical Center of Japan, Tokyo 162-8655, Japan and also with the Department of Pharmacokinetics and Pharmacodynamics, Tokyo Medical and Dental University Graduate School, Tokyo 113-8519, Japan.

*K. Yamamoto is with the Research Institute, International Medical Center of Japan, Tokyo 162-8655, Japan and also with the Department of Pharmacokinetics and Pharmacodynamics, Tokyo Medical and Dental University Graduate School, Tokyo 113-8519, Japan (e-mail: backen@ri.imcj.go.jp).

Digital Object Identifier 10.1109/TNB.2007.891883

[1]Supplemental movies: This information is available free of charge via the Internet at http://www.geocities.jp/backenlab/.

proline) as follows: aqueous dipeptide solution in ethanol was dripped into the QD-TOPO solution in tetrahydrofuran (Wako Pure Chemical Industries, Ltd.; Osaka, Japan) and then the mixture was warmed up to 85 °C, and refluxed for 12 h. After the reaction, NaOH solution (pH10) was added and the mixture was heated at 90 °C to remove the contained tetrahydrofuran by evaporation. The obtained ACQDs solution was then purified and concentrated with an ultrafiltration membrane (Amicon Ultra-4, Millipore Corporation, Billerica, MA). The final purification was performed with a gel filtration column (MicroSpin G-25 Columns, Amersham Bioscience, San Francisco, CA).

C. Vitrectomy

A standard 3-port pars plana vitrectomy was performed on a porcine eye (6 months old) mounted in a human head model using a 20-gauge vitreous cutter and a hand-held light pipe. Sclerotomies were placed 3.5 mm posterior to the corneal limbus in the superotemporal, superonasal and inferotemporal quadrants. The infusion cannula was sutured in the inferotemporal sclerotomy site. The 20-gauge hand-held light pipe was inserted first into the vitreous cavity, then the vitreous cutter was inserted. Finally, the vitreous was cut and eliminated by vitreous cutter. The porcine eye stained with QDs will be an excellent vitrectomy training device as a virtual human eye for ophthalmology residents.

III. RESULTS

A. Detection of Weiss Ring With ACQDs

We evaluated whether ACQDs are effective to detect the Weiss ring (WR). The WR is a ring-shaped structure of posterior vitreous in the vitreous cavity, formerly attached with the optic nerve disc (Fig. 1). Aging accelerates the liquefaction of the vitreous and the posterior vitreous detachment (PVD) from the retina. But posterior vitreous attaches with the optic nerve disc strongly, then the final step of posterior vitreous detachment forms the WR structure. Therefore, in clinical situations, the eye with WR is regarded as the eye with PVD. It is very important to diagnose PVD. If posterior vitreous attaches with the retina, blood vessels of the retina enter directly into the vitreous. Then, proliferative eye diseases deteriorate rapidly. However, it is difficult to detect the PVD in clinical situations. Since the white light used for inspection reflects from the retina, the contrast of the retina and WR is indistinguishable.

To visualize the transparent vitreous, we injected the ACQDs (red emitting 640 nm) into the vitreous cavity of an enucleated aged and a young porcine eye with a 27-gauge needle via pars plana of the ciliary body (Fig. 2). In order to examine the effect of ACQDs, the efficiency of ACQDs was compared with that of a conventional dye TA. Just after the injection of ACQDs, they dispersed into the vitreous cavity (see supplementary movie S1). The fluorescence reflection from ACQDs made it possible to observe the structure in the posterior side of the vitreous cavity. The striking contrast enables us to observe vitreous structures by a slit lamp microscopy without any difficulty [Fig. 2(a), 2(b)]. Consequently the details of the status of vitreous are detected easily because ACQDs can be excited by a white lump which is commonly used as a light source. In contrast, TA fails to visualize the subtle vitreous structures because it is turbid in vitreous [Fig. 2(c)]. As a result, ACQDs enable us to detect details of the status of the vitreous at striking contrast.

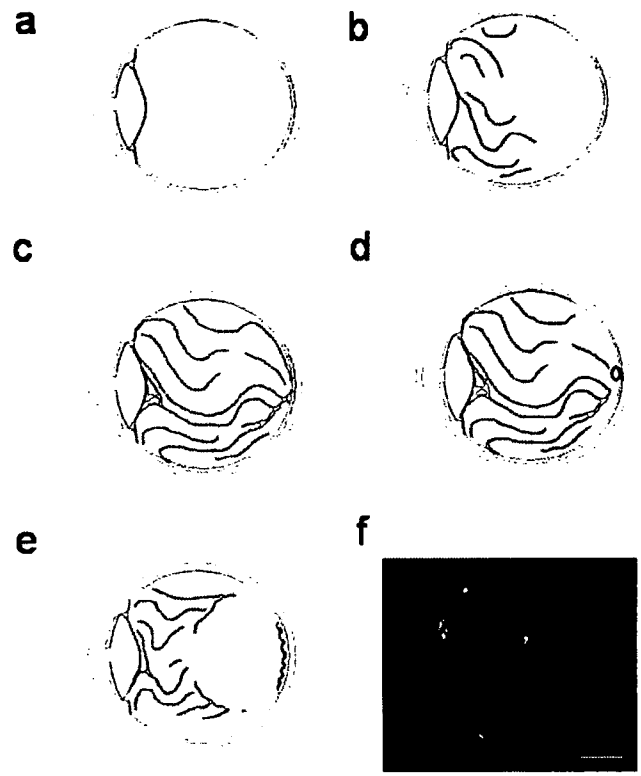

Fig. 1. Age-related change of vitreous lesion. (a) The vitreous of the neonatal eye. The vitreous cavity is uniform and the fiber of the vitreous gel (collagen and hyarulonate with water) exists in the radial pattern. (b) The vitreous of the young eye. The tractus was formed in former vitreous whereas the structure of the latter cavity still remained. (c) The vitreous of the aged eye. The tractus formation was expanded to all the vitreous cavity. (d) The PVD formed eye. Liquefaction of the vitreous gel started. The red circle indicates the WR. (e) The structure of the PVD-developed eye. In some cases, posterior vitreous gel located in the latter cavity. (f) Distribution of ACQDs in the vitreous. ACQD solution (200 μL) was injected into the vitreous cavity and then the whole eye was frozen. The cryosection of the whole eyeball was observed on a fluorescent microscopy equipped with a cooled CCD camera. The illustration of the eye structure was superimposed onto the photo image. The bar indicates 10 mm.

B. ACQDs With a Vitreous Staining Device for Vitrectomy

This result encouraged us to use ACQDs as an imaging agent for vitrectomy. There are few imaging agents used for vitrectomy, and it is quite difficult to remove all vitreous lesions without making new iatrogenic lesions. To demonstrate the efficiency of ACQDs, a vitrectomy on the porcine eye was performed under a surgical microscopy and compared with these conventional organic probes. First we injected the organic fluorescent probes and evaluated them. Fluorescein, which emits yellow-green fluorescence, is too bright in the vitreous to discern between the optical reflection from the retina and vitreous lesion [Fig. 3(a)]. Another organic dye, indocyanine green, which is used for diagnosis of age-related macular degeneration, is an infrared fluorescent probe and not suitable for dye for vitrectomy [Fig. 3(b)]. In contrast, the ACQD-probe

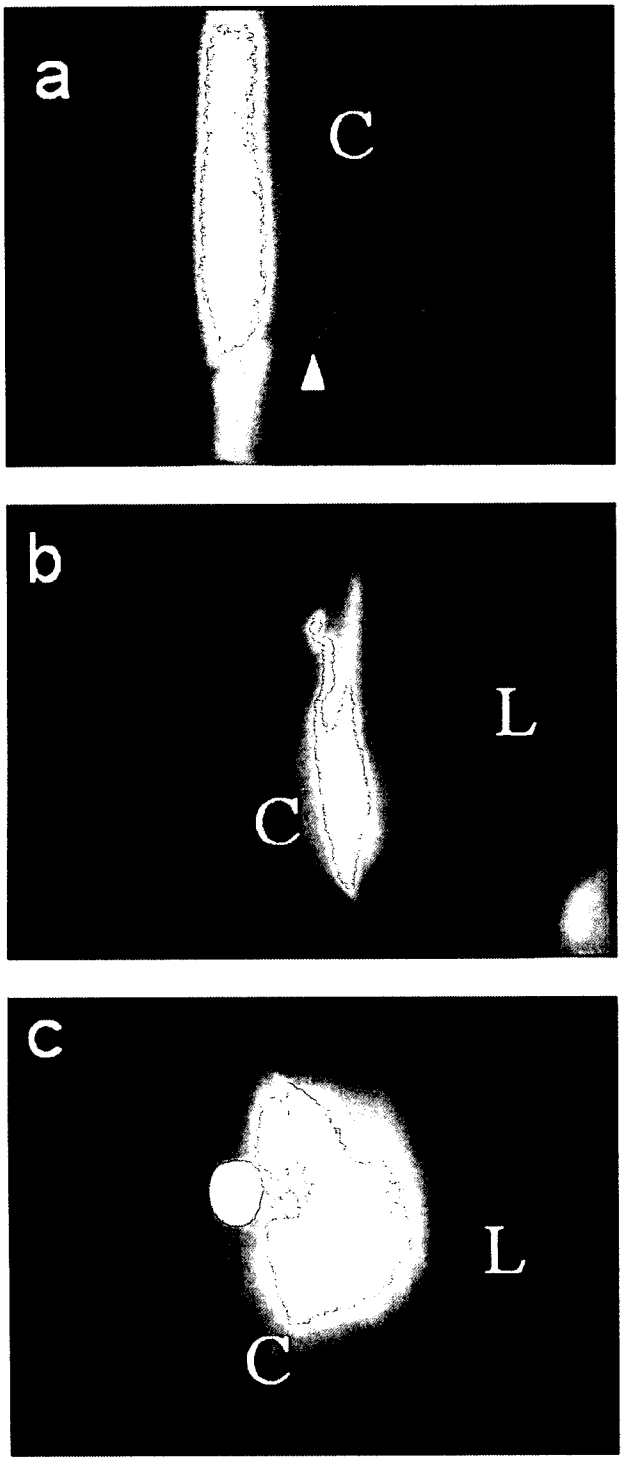

Fig. 2. ACQDs enable us to visualize the structure in vitreous at striking contrast. (a) The vitreous of the aged eye was observed with a slit lamp microscopy using ACQDs. The arrowhead indicates the WR. (b) The anterior view of the young eye with direct illumination showed the iatrogenic cavity in vitreous located just behind the lens. Fluorescence emitted from ACQD reflected the structures of vitreous and enabled us to observe easily. (c) The injection of triamcinolone acetonide (TA) identified the structure of the vitreous poorly because the particle of TA was very big and turbid. C: iatrogenic cavity; L: lens.

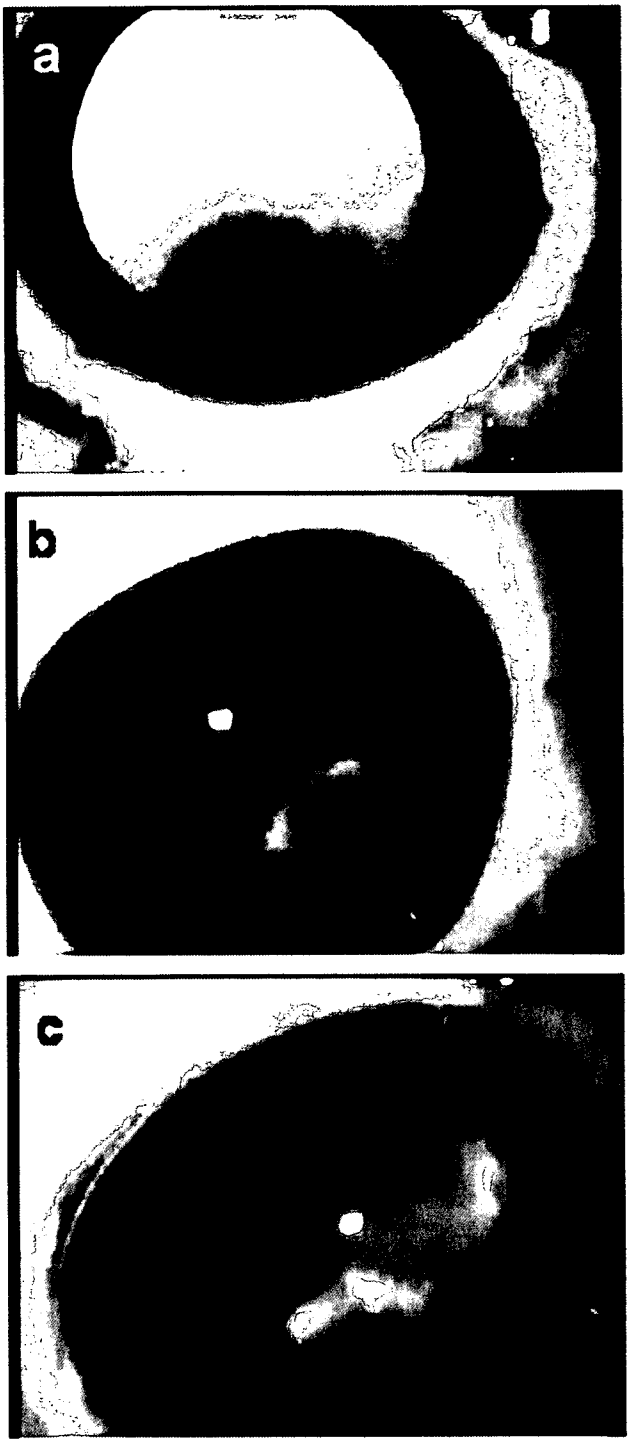

Fig. 3. Comparison of ACQDs and conventional organic dyes to perform vitrectomy. A vitrectomy of the porcine eye (6 months old) was performed with: (a) fluorescein sodium; (b) indocyanine green; and (c) ACQDs. (a) The brighter fluorescence emitted from fluorescein sodium made it harder to observe the vitreous. (b) Indocyanine green illuminates only the narrow range. (c) ACQDs can visualize the structure of vitreous at a striking contrast. In the case of vitrectomy, transparent vitreous was stained. Then these dyes were excited by light guide to make a striking contrast in vitreous.

is an efficient dye for vitrectomy. Transparent vitreous stained red with ACQDs made it easy to cut and aspirate the target lesion completely (see supplementary movie S2). The translucent red fluorescence from ACQDs enabled us to confirm the

location of other structures such as the retina, blood vessels of retina, and ciliary body, and that resulted in reducing the risk to injure other eye structures [Fig. 3(c)]. In addition, the shaving of the surface of retina was required to complete vitrectomy. Visible and translucent ACQDs make it possible to complete vitrectomy successfully.

IV. Discussions

Currently, colloidal nanocrystal quantum dots (QDs) are widely used in biological and medical study because QDs are attractive fluorophores for multicolor imaging due to their broad absorption and narrow emission spectra, and brighter and higher photostability than organic dyes. Many advanced improvements on surface modification of QDs enable us to promote a lot of biological experiments. We previously reported that QDs were applied to some biological experiments; long-term multicolor cell imaging in live cells [16]–[20], and even in cancer immunotherapy with QDs [21], [22]. In addition, this study suggests that ACQDs are excellent imaging agents to visualize invisible vitreous in clinical situations.

Although there are some concerns about the safety of ACQDs [23], we previously reported that the ACQD-covering molecules controlled their cytotoxicity unless the core structure of QDs was broken [24]. In vitrectomy, the ACQDs in vitreous were depleted completely by aspiration; then residual ACQDs were thought to be quite little after vitrectomy. We anticipate that the new imaging agent and method will be used broadly, and that vitreous conditions will be diagnosed and understood easily and fully in usual clinical situations. And safe vitrectomy can be completed by any ophthalmic surgeons. With the development of *in vivo* imaging systems, ACQD techniques may contribute not only to analyzing the mechanism of the side effect but to producing new medicines in the future.

In this paper, we examined study with QDs medicine of CdSe/ZnS *in vivo*. Derfus *et al.* [25] reported that core-shell typed QDs irradiated with ultraviolet more than 8 h showed the cytotoxicity by the leaked Cd^{2+} ion, but no sign of cytotoxicity in case of 1 hr exposure. We also found no sign of cytotoxicity under the condition of our *in vitro* experiments with some epithelial cell lines. In addition, no significant change was observed in vitreous after a wide range of doses of the ACQDs *in vivo*. This result is consistent with the report of Derfus *et al.* QDs made from metals that could generate toxic ions might exhibit cytotoxicity in some unexpected cases. Warner *et al.* reported the method of the production of silicon dots [26]. Further study will make possible clinical applications of QDs made from materials more suitable for safety, such as silicon.

V. Conclusion

ACQDs are much better imaging reagents in vitreous compared with some conventional dyes used in clinical situations. ACQDs will enable ophthalmic surgeons to perform more reliable vitrectomy, resulting in an easy and safe surgery method. Consequently, an ACQD-oriented vitreous system will light the way for ophthalmological science and clinical treatment.

Acknowledgment

The authors would like to thank Japan Alcon Corporation (Tokyo, Japan) for kindly providing a three port pars plana vitrectomy system. The authors are also grateful to Dr. M. Nii (Tokushima A. F. F. Technology Center, Tokushima Japan) for kindly providing an aged porcine eye.

References

[1] J. G. F. Worst and L. I. Los, *Cisternal Anatomy of the Vitreous.* The Hague, The Netherlands: Kugler, 1995.
[2] J. Sebag, "Anomalous posterior vitreous detachment: a unifying concept in vitreo-retinal disease," *Grafe's Arch. Clin. Exp. Ophthalmol.*, vol. 242, pp. 690–698, 2004.
[3] ——, "Age-related changes in human vitreous structure," *Graefes Arch Clin Exp Ophthalmol*, vol. 225, pp. 89–93, 1987.
[4] ——, "Seeing the invisible: the challenge of imaging vitreous," *J. Biomed. Opt.*, vol. 9, pp. 38–46, 2004.
[5] A. Kakehashi, S. Ishiko, S. Konno, J. Akiba, M. Kado, and A. Yoshida, "Observing the posterior vitreous by means of the scanning laser ophthalmoscope," *Arch. Ophthalmol.*, vol. 113, pp. 558–560, 1995.
[6] D. J. Coleman, S. W. Daly, A. Atencio, H. O. Lloyd, and R. H. Silverman, "Ultrasonic evaluation of the vitreous and retina," *Semin. Ophthalmol.*, vol. 13, pp. 210–218, 1998.
[7] T. Hikichi, J. Akiba, A. Kakehashi, and A. Yoshida, "Vitreous observation using a CCD camera and a computerized unit for image processing and storage," *Retina*, vol. 15, pp. 505–507, 1995.
[8] K. Mori and S. Yoneya, "Enhanced documentation of slit-lamp images of the human vitreous stained with fluorescein sodium," *Ophthalmic Surg. Lasers Imaging*, vol. 35, pp. 233–238, 2004.
[9] W. Drexler, U. Morgner, R. K. Ghanta, F. X. Kartner, J. S. Schuman, and J. G. Fujimoto, "Ultrahigh-resolution ophthalmic optical coherence tomography," *Nature Med.*, vol. 7, pp. 502–507, 2001.
[10] M. W. Johnson, "Improvements in the understanding and treatment of macular hole," *Curr. Opin. Ophthalmol.*, vol. 13, pp. 152–160, 2002.
[11] V. Tanner, D. S. Chauhan, T. L. Jackson, and T. H. Williamson, "Optical coherence tomography of the vitreoretinal interface in macular hole formation," *Br J Ophthalmol*, vol. 85, pp. 1092–1097, 2001.
[12] H. Terasaki, Y. Miyake, M. Mori, T. Suzuki, and M. Kondo, "Fluorescein angiography of extreme peripheral retina and rubeosis iridis in proliferative diabetic retinopathy," *Retina*, vol. 19, pp. 302–308, 1999.
[13] J. K. Challa, M. C. Gillies, P. L. Penfold, J. F. Gyory, A. B. Hunyor, and F. A. Billson, "Exudative macular degeneration and intravitreal triamcinolone: 18 month follow up," *Aust. N. Z. J. Ophthalmol.*, vol. 26, pp. 277–281, 1998.
[14] J. B. Jonas, I. Kreissig, and R. Degenring, "Intraocular pressure after intravitreal injection of triamcinolone acetonide," *Br. J. Ophthalmol.*, vol. 87, pp. 24–27, 2003.
[15] D. M. Moshfeghi, P. K. Kaiser, I. U. Scott, J. E. Sears, M. Benz, J. P. Sinesterra, R. S. Kaiser, S. J. Bakri, R. K. Maturi, J. Belmont, P. M. Beer, T. G. Murray, H. Quiroz-Mercado, and W. F. Mieler, "Acute endophthalmitis following intravitreal triamcinolone acetonide injection," *Amer. J. Ophthalmol.*, vol. 136, pp. 791–796, 2003.
[16] M. Dahan, S. Levi, C. Luccardini, P. Rostaing, B. Riveau, and A. Triller, "Diffusion dynamics of glycine receptors revealed by single-quantum dot tracking," *Science*, vol. 302, pp. 442–445, 2003.
[17] E. R. Goldman, A. R. Clapp, G. P. Anderson, H. T. Uyeda, J. M. Mauro, I. L. Medintz, and H. Mattoussi, "Multiplexed toxin analysis using four colors of quantum dot fluororeagents," *Anal. Chem.*, vol. 76, pp. 684–688, 2004.
[18] A. Hoshino, K. Fujioka, T. Oku, S. Nakamura, M. Suga, Y. Yamaguchi, K. Suzuki, M. Yasuhara, and K. Yamamoto, "Quantum dots targeted to the assigned organelle in living cells," *Microbiol. Immunol.*, vol. 48, pp. 985–994, 2004.
[19] J. K. Jaiswal, H. Mattoussi, J. M. Mauro, and S. M. Simon, "Long-term multiple color imaging of live cells using quantum dot bioconjugates," *Nature Biotechnol.*, vol. 21, pp. 47–51, 2003.
[20] A. Hoshino, K. Hanaki, K. Suzuki, and K. Yamamoto, "Applications of T-lymphoma labeled with fluorescent quantum dots to cell tracing markers in mouse body," *Biochem. Biophys. Res. Commun.*, vol. 314, pp. 46–53, 2004.
[21] X. Gao, Y. Cui, R. M. Levenson, L. W. Chung, and S. Nie, "In vivo cancer targeting and imaging with semiconductor quantum dots," *Nature Biotechnol.*, vol. 22, pp. 969–976, 2004.

[22] E. B. Voura, J. K. Jaiswal, H. Mattoussi, and S. M. Simon, "Tracking metastatic tumor cell extravasation with quantum dot nanocrystals and fluorescence emission-scanning microscopy," *Nature Med.*, vol. 10, pp. 993–998, 2004.
[23] R. Hardman, "A toxicologic review of quantum dots: toxicity depends on physicochemical and environmental factors," *Environ. Health Perspect.*, vol. 114, pp. 165–172, 2006.
[24] A. Hoshino, K. Fujioka, T. Oku, M. Suga, Y. F. Sasaki, T. Ohta, M. Yasuhara, K. Suzuki, and K. Yamamoto, "Physicochemical properties and cellular toxicity of nanocrystal quantum dots depend on their surface modification," *Nano Lett.*, vol. 4, pp. 2163–2169, 2004.
[25] A. M. Derfus, W. C. W. Chan, and S. N. Bhatia, "Probing the cytotoxicity of semiconductor quantum dots," *Nano Lett.*, vol. 4, pp. 11–18, 2004.
[26] J. H. Warner, A. Hoshino, K. Yamamoto, and R. D. Tilley, "Water-soluble photoluminescent silicon quantum dots," *Angew. Chem. Int. Ed. Engl.*, vol. 44, pp. 4550–4554, 2005.

Satoru Yamamoto was born in Japan on August 30, 1964. He received the M.D. degree from the School of Medicine, Mie University, Japan, in 1992. He also studied at Wilmer Eye Institute, Johns Hopkins University, Baltimore, MD.

He is currently Director of the Department of Ophthalmology, Yokohama Sakae Kyousai Hospital, Yokohama, Japan. In university, he studied ophthalmology and especially skills in ophthalmic surgery. He is currently interested in quantum dots and their clinical applications in the field of ophthalmology.

Dr. Yamamoto is a member of the American Academy of Ophthalmology (AAO) and the Association for Research in Vision and Ophthalmology (ARVO), and a Fellow Researcher at the International Clinical Research Center, International Medical Center of Japan (IMCJ).

Noriyoshi Manabe photograph and biography not available at the time of publication.

Kouki Fujioka, photograph and biography not available at the time of publication.

Akiyoshi Hoshino, photograph and biography not available at the time of publication.

Kenji Yamamoto, photograph and biography not available at the time of publication.

The p85α Regulatory Subunit of Class IA Phosphoinositide 3-Kinase Regulates β-Selection in Thymocyte Development[1]

Fumiko Shiroki,* Satoshi Matsuda,*† Tomomitsu Doi,*† Mari Fujiwara,*† Yoshito Mochizuki,* Takashi Kadowaki,†‡ Harumi Suzuki,*§ and Shigeo Koyasu[2]*†

We examined the role of class IA PI3K in pre-TCR controlled β-selection and TCR-controlled positive/negative selection in thymic development. Using mice deficient for p85α, a major regulatory subunit of the class IA PI3K family, the role of class IA PI3K in β-selection was examined by injection of anti-CD3ε mAb into p85α$^{-/-}$Rag-2$^{-/-}$ mice, which mimics pre-TCR signals. Transition of CD4$^-$CD8$^-$ double-negative (DN) to CD4$^+$CD8$^+$ double-positive (DP) thymocytes triggered by anti-CD3ε mAb was significantly impaired in p85α$^{-/-}$Rag-2$^{-/-}$ compared with p85α$^{+/-}$Rag-2$^{-/-}$ mice. Furthermore, DP cell numbers were lower in p85α$^{-/-}$DO11.10/Rag-2$^{-/-}$ TCR-transgenic mice than in DO11.10/Rag-2$^{-/-}$ mice. In addition, inhibition by IC87114 of the major class IA PI3K catalytic subunit expressed in lymphocytes, p110δ, blocked transition of DN to DP cells in embryonic day 14.5 fetal thymic organ culture without affecting cell viability. In the absence of phosphatase and tensin homolog deleted on chromosome 10, where class IA PI3K signals would be amplified, the DN to DP transition was accelerated. In contrast, neither positive nor negative selection in Rag-2$^{-/-}$TCR-transgenic mice was perturbed by the lack of p85α. These findings establish an important function of class IA PI3K in the pre-TCR-controlled developmental transition of DN to DP thymocytes. ***The Journal of Immunology*****, 2007, 178: 1349–1356.**

T cell development in the thymus is a highly controlled process beginning with the most immature thymocyte, termed CD4$^-$CD8$^-$ double-negative (DN)[3] (1–3). The DN progenitors can be subdivided into four different stages based on their CD44 and CD25 expression patterns. The earliest progenitors are CD44$^+$CD25$^-$ (DN1) cells, followed by CD44$^+$CD25$^+$, CD44$^-$CD25$^+$, and CD44$^-$CD25$^-$ (DN2–4, respectively) cells. After successful rearrangement of the TCRβ, the CD44$^-$CD25$^+$ (DN3) cells express a pre-TCR on their surface made up of the TCRβ protein and a pTα. After passing the first T cell developmental checkpoint, namely β-selection, DN3 cells make the transition to the CD4$^+$CD8$^+$ double-positive (DP) stage. This transition includes cell proliferation triggered by signals through the pre-TCR. The pre-TCR also triggers rearrangement of the *TCRα* gene, leading to the expression of TCRαβ heterodimers on DP cells. These cells then go through a second checkpoint, termed positive and negative selection. DP cells receiving weak signals through the TCR survive and differentiate into mature CD4$^+$ or CD8$^+$ single-positive (SP) cells (positive selection), whereas those receiving strong signals are eliminated (negative selection). Furthermore, those incapable of recognizing appropriate MHC molecules fail to receive the TCR signal and are also eliminated (death by neglect) (1–3).

PI3Ks are lipid kinases that specifically phosphorylate the D3 position of the inositol ring of phosphatidylinositol (PI) species (reviewed in Refs. 4–7). PI3Ks are activated through a variety of extracellular stimuli and promote assembly of signaling complexes at the plasma membrane. PI(3,4)P_2 and PI(3,4,5)P_3, products of PI3Ks, recruit specific signaling proteins containing a pleckstrin homology domain that selectively binds 3-phosphoinositides. These signaling proteins include phosphoinositide-dependent kinase 1 (PDK1), Akt, and Vav1 and are involved in a wide range of cellular processes such as cell metabolism, cell cycle progression and survival. PI3K-signaling pathways are counteracted by phosphatase and tensin homologue deleted on chromosome 10 (Pten), a 3-phosphoinositide-specific lipid phosphatase.

The class IA PI3Ks are heterodimeric proteins composed of a catalytic (p110α, p110β, or p110δ) and a regulatory (p85α, p55α, p50α, p85β, or p55γ) subunit and are activated mostly downstream of protein tyrosine kinases (4–7). Each regulatory subunit can interchangeably associate with different catalytic subunits and shows a unique tissue distribution. p85α, a product encoded by the *Pik3r1* gene, is the major regulatory subunit of class IA PI3Ks in most types of cells including immune cells. The *Pik3r1* gene encodes two alternative splicing forms in addition to p85α, p55α, and p50α. Mice lacking p85α alone or mice lacking all products encoded by the *Pik3r1* gene (p85α, p55α, and p50α) show comparable immune phenotypes such that B cell development and activation are impaired while T cell functions are apparently unaffected (8–10). In contrast, mice lacking the p85β regulatory subunit or transgenic (tg) mice

*Department of Microbiology and Immunology, Keio University School of Medicine, Tokyo, Japan; †Core Research for Evolutional Science and Technology, Japan Science and Technology Agency, Saitama, Japan; ‡Department of Metabolic Diseases, Graduate School of Medicine, University of Tokyo, Tokyo, Japan; and §Department of Pathology, Research Institute, International Medical Center of Japan, Tokyo, Japan

Received for publication July 12, 2006. Accepted for publication November 16, 2006.

The costs of publication of this article were defrayed in part by the payment of page charges. This article must therefore be hereby marked *advertisement* in accordance with 18 U.S.C. Section 1734 solely to indicate this fact.

[1] This work was supported by the Mitsubishi Foundation, a Keio University Special Grant-in-Aid for Innovative Collaborative Research Project, a Grant-in-Aid for Scientific Research for Young Scientist (16790293 to S.M.) from the Japan Society for the Promotion of Science, a Grant-in-Aid for Scientific Research on Priority Areas (14021110 to S.K. and 16043248 to S.M.), a National Grant-in-Aid for the Establishment of a High-Tech Research Center in a private university, and a Scientific Frontier Research Grant from the Ministry of Education, Culture, Sports, Science and Technology, Japan.

[2] Address correspondence and reprint requests to Dr. Shigeo Koyasu, Department of Microbiology and Immunology, Keio University School of Medicine, 35 Shinanomachi, Shinjuku-ku, Tokyo 160-8582, Japan. E-mail address: koyasu@sc.itc.keio.ac.jp

[3] Abbreviations used in this paper: DN, double negative; DP, double positive; SP, single positive; tg, transgenic; PI, phosphatidylinositol; Pten, phosphatase and tensin homolog deleted on chromosome 10; PDK, phosphoinositide-dependent kinase; 7AAD, 7-aminoactinomycin D; FTOC, fetal thymic organ culture.

expressing a p85α-binding domain derived from the p110α catalytic subunit show some phenotypes in T cells rather than B cells (11, 12). Among the catalytic subunits of the class IA PI3Ks, inactivation of p110δ, a catalytic subunit expressed predominantly in lymphocytes, impairs Ag-induced proliferation of both T and B cells (13). Interestingly, however, knockout studies have shown that the lack of p110δ leads to defects in the development and function of B cells but not T cells (14, 15).

There has been some indirect evidence suggesting the importance of PI3Ks in early T cell development. For example, T cell-specific deletion of Pten resulted in an increase in thymocyte numbers and allowed transition of DN thymocytes to DP in CD3γ$^{-/-}$ mice (16). Introduction of a constitutively active form of Akt1 along with TCRβ efficiently induced DP cells from Rag-2$^{-/-}$ DN3 cells in an OP9-DL1 culture system (17). Furthermore, reduced expression of PDK1, which functions upstream of Akt, resulted in impaired thymocyte expansion and developmental arrest at DN4 (18). These results strongly suggest the involvement of PI3Ks in T cell development. More recent papers suggested the role of p110γ and p110δ in early thymocyte differentiation (19, 20). To directly elucidate the functions of PI3Ks in β-selection, we used Rag-2$^{-/-}$ mice in which β-selection can be directly examined in vivo by injection of anti-CD3ε mAb. We also assessed the role of p85α in negative as well as positive selection in the thymus using TCR-tg mice on a Rag-2$^{-/-}$ background where no endogenous TCR is involved in the selection procedures. Our results demonstrate here that class IA PI3Ks regulate the β-selection process but not positive and negative selection processes.

Materials and Methods

Mice

p85α$^{-/-}$ mice (21) were backcrossed to BALB/c or C57BL/6 mice for 12 generations before intercrossing heterozygous mice. The colony has been maintained by mating p85α$^{+/-}$ female mice and p85α$^{-/-}$ male mice, because p85α$^{-/-}$ females are virtually sterile. Rag-2$^{-/-}$ mice on a BALB/c background, Rag-2$^{-/-}$ mice on a C57BL/6 background, DO11.10/Rag-2$^{-/-}$ mice on a BALB/c background, Cyt5CC7/Rag-2$^{-/-}$ mice on a B10.A background, P14/Rag-2$^{-/-}$ mice on a C57BL/10 background, and Lck-Cre-tg mice on a C57BL/6 background were obtained from Taconic Farms. p85α$^{-/-}$Rag-2$^{-/-}$ mice were generated by mating p85α$^{-/-}$ and Rag-2$^{-/-}$ mice on a BALB/c background. p85α$^{-/-}$ mice were also crossed with DO11.10/Rag-2$^{-/-}$, Cyt5CC7/Rag-2$^{-/-}$, or P14/Rag-2$^{-/-}$ mice to generate various TCR-tg mice on a p85α$^{-/-}$Rag-2$^{-/-}$ background. Resulting p85α$^{-/-}$DO11.10/Rag-2$^{-/-}$, p85α$^{-/-}$Cyt5CC7/Rag-2$^{-/-}$, and p85α$^{-/-}$P14/Rag-2$^{-/-}$ mice were on BALB/c, B10.A, and C57BL/6 backgrounds, respectively. To generate Rag-2$^{-/-}$ mice with a T cell-specific Pten deficiency, Pten$^{flox/flox}$ mice on a C57BL/6 background (22) were crossed with Rag-2$^{-/-}$ mice on a C57BL/6 background. These mice were further crossed with Lck-Cre-tg mice on a C57BL/6 background. In this paper Lck-Cre/Pten$^{flox/flox}$ mice and Pten$^{flox/flox}$ mice were described as Pten$^{-/-}$ and Pten$^{+/+}$ mice, respectively. All mice were maintained at Taconic Farms or in our animal facility under specific pathogen-free conditions. All experiments were performed in accordance with our institutional guidelines.

In vivo administration of anti-CD3ε mAb and antigenic peptide

Anti-CD3ε mAb (2C11) was immunoaffinity purified from culture supernatant of a hybridoma in our laboratory. A total of 75 μg of 2C11 was delivered by i.p. injection into Rag-2$^{-/-}$ mice to examine the DN to DP transition (23). Sera were prepared from each mouse 2 h after injection and were analyzed for serum Ab titer by ELISA to confirm that the Ab was properly injected. Thymocytes were analyzed at various time points after injection. DO11.10/Rag-2$^{-/-}$ mice were i.v. injected with 50 μg of $OVA_{323-339}$ peptide every 24 h three times. Thymocytes were analyzed 72 h after the first injection.

Flow cytometry and cell sorting

FITC-conjugated anti-CD8α (53-6) and biotinylated anti-CD3ε (2C11) mAbs were produced in our laboratory. FITC-conjugated anti-CD44 (IM7), PE-conjugated anti-CD4 (GK1.5) and anti-CD25 (3C7), allophycocyanin-CyChrome 7 conjugated anti-CD4 (GK1.5), and biotinylated anti-CD2 (RM2-5) mAbs were purchased from BD Biosciences. Biotinylated anti-Vβ2 (B20.6), anti-Vβ3 (KJ25), anti-Vβ7 (TR310), anti-Vβ8 (F23.1), anti-Vβ9 (MR10-2), anti-Vβ12 (MR11-1), anti-Vβ14 (14-2) mAbs were purchased from BD Pharmingen. Binding of biotinylated mAbs was detected with streptavidin-allophycocyanin (BD Biosciences). After incubation with anti-FcγR mAb (2.4G2) to block nonspecific binding of mAbs, cells were stained with the designated Abs in HBSS with 0.1% BSA and were subjected to analysis on a FACSCalibur using the CellQuest program (BD Biosciences). Dead cells were gated out using 7-aminoactinomycin D (7AAD).

To purify DN subsets, DN cells were first enriched by depletion of DP and SP cells using anti-CD8α-coated magnetic beads with an AutoMACS (Miltenyi Biotec). DN cells were then stained with FITC-conjugated anti-CD44, PE-conjugated anti-CD25, allophycocyanin-cychrome-7-conjugated anti-CD4, biotinylated anti-CD3ε mAb, followed by staining with streptavidin-allophycocyanin, and 7AAD. After gating on the CD4 and CD3ε DN population, cells were sorted into DN1–4 populations according to CD44 and CD25 expression profiles on a FACSAria (BD Biosciences). DP (CD8$^+$CD4$^+$) cells were also isolated using a FACSAria. The sorted populations were reanalyzed on a FACSAria for their purity and were found to be >99% pure.

Western blot analysis

Anti-p85^{PAN} Ab recognizing class IA PI3K regulatory subunits (p85α, p55α, p50α, p85β, and p55γ) was purchased from Upstate Biotechnology. Anti-p110δ (H-119) Ab and anti-Pten (H-19) Ab were purchased from Santa Cruz Biotechnology. Anti-phospho-Akt (Ser^{473}) (193H12) mAb and anti-Akt Ab were purchased from Cell Signaling Technology. Cells were lysed in a lysis buffer solution (1% Nonidet P-40, 20 mM Tris-HCl (pH 7.5), 2 mM EGTA, 10 mM NaF, 12.5 mM β-glycerophosphate, 1 mM benzamidine, 1% aprotinin, and 2 mM DTT). The cell lysates were applied to SDS-PAGE and were transferred to polyvinyldifluoride membranes to perform Western blot analysis. Reactive proteins were visualized with ECL chemiluminescent substrates (NEN or GE Healthcare Bio-Sciences). To normalize sample loading, membranes were stripped by a stripping buffer solution (62.5 mM Tris-HCl (pH 6.8), 2% SDS, and 100 mM 2-ME) and subsequently reblotted with anti-ERK2 Ab (Santa Cruz Biotechnology).

Miscellaneous

A p110δ-selective inhibitor IC87114 (24) was provided by ICOS. To confirm the efficacy of IC87114, purified T cells were preincubated for 20 min at 37°C with or without IC87114 and then were stimulated with a mixture of anti-CD3ε and anti-CD28 mAb and goat anti-hamster IgG Ab (MP Biomedicals) (10 μg/ml, respectively) at 37°C for 5 min. Anti-CD28 mAb (37.51) was also immunoaffinity purified from culture supernatant of a hybridoma in our laboratory. T cells were purified from total splenocytes using anti-CD4 and anti-CD8α-coated magnetic beads with an AutoMACS (Miltenyi Biotec) (purity of the cells was >95%).

Fetal thymic organ culture (FTOC) was performed as follows. After dissection of day 14.5 fetuses obtained from timed pregnant mice, individual thymic lobes were placed on a Millipore filter (Whatman) placed on a sponge soaked in RPMI 1640 (Sigma-Aldrich) supplemented with 1% penicillin-streptomycin, 2 mM glutamine, 1% sodium pyruvate, 1% MEM nonessential amino acid, 10 mM HEPES (all from Invitrogen Life Technologies), and 10% FCS (HyClone) in 24-well plates. Plates were incubated at 37°C in 5% CO_2 in air and 95% humidity. After 5 days of incubation, cells were recovered and analyzed.

Statistical analysis was performed with the Mann-Whitney U test. Values of $p < 0.05$ were considered significant. Cell numbers and ratios of the thymic population were calculated for independent experiments performed in duplicate or triplicate.

Results

Pre-TCR signal-induced transition of DN to DP thymocytes in Rag-2$^{-/-}$ mice is delayed in the absence of p85α

We examined the role of p85α in early thymocyte development with anti-CD3ε mAb injection into Rag-2$^{-/-}$ mice. Although thymocytes of Rag-2$^{-/-}$ mice are arrested at the DN3 stage due to the lack of TCRβ rearrangement, pre-TCR signals can be generated in Rag-2$^{-/-}$ mice by injection of anti-CD3ε mAb. This mimics β-selection and results in transition from the DN3 through DN4 to DP stage (termed DN3 to DP transition) and cell expansion during such transition (23). To determine whether p85α is involved in the

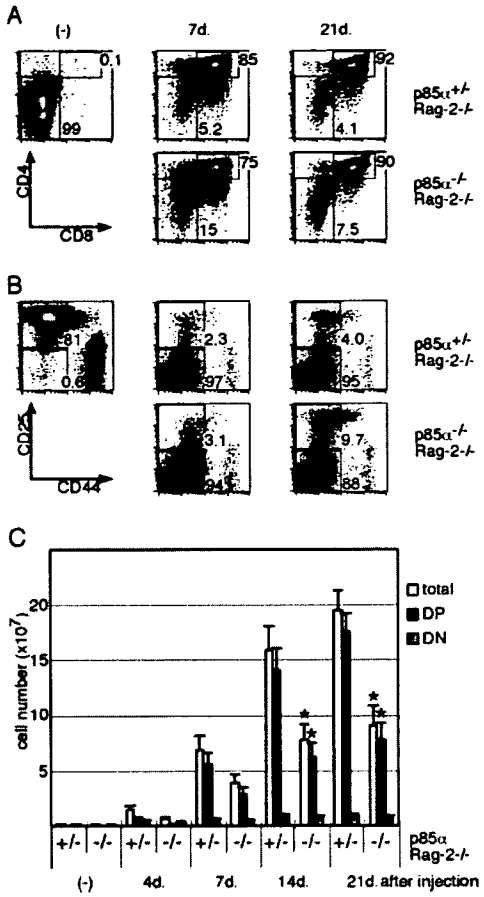

FIGURE 1. DP cell transition upon anti-CD3ε mAb stimulation delays in p85α$^{-/-}$Rag-2$^{-/-}$ mice compared with p85α$^{+/-}$Rag-2$^{-/-}$ mice. *A* and *B*, CD8/CD4 and CD44/CD25 surface phenotypes were examined in p85α$^{-/-}$Rag-2$^{-/-}$ and p85α$^{+/-}$Rag-2$^{-/-}$ mice at the indicated times after i.p. injection of anti-CD3ε mAb. Numbers are the percentages of each population. The lack of p85α had no effect on the expression levels of CD3ε on Rag-2$^{-/-}$ thymocytes (data not shown). *C*, Total thymocyte numbers and absolute numbers of DP and DN cells are shown as mean ± SEM in p85α$^{-/-}$Rag-2$^{-/-}$ and p85α$^{+/-}$Rag-2$^{-/-}$ mice before anti-CD3ε mAb stimulation and at the indicated days after injection (n = 10–13, except for 4 days where seven mice were analyzed). At 14 and 21 days after injection, thymocyte numbers as well as DP cell numbers in p85α$^{-/-}$Rag-2$^{-/-}$ mice are significantly lower than those in p85α$^{+/-}$Rag-2$^{-/-}$ mice (*, $p < 0.01$).

pre-TCR-mediated transition from DN3 to DP, we injected anti-CD3ε mAb into p85α$^{-/-}$Rag-2$^{-/-}$ mice and p85α$^{+/-}$Rag-2$^{-/-}$ littermate controls. Thymocytes of p85α$^{-/-}$Rag-2$^{-/-}$ mice are also arrested at the DN3 stage as observed in Rag-2$^{-/-}$ mice. Anti-CD3ε mAb-induced transition from the DN3 to DP stage was significantly impaired in p85α$^{-/-}$Rag-2$^{-/-}$ mice as compared with control mice (Fig. 1). Thymocyte expansion during transition to DP cells was also affected in p85α$^{-/-}$Rag-2$^{-/-}$ mice, as total thymocyte numbers as well as DP cell numbers were significantly lower in p85α$^{-/-}$Rag-2$^{-/-}$ mice than those of control mice (Fig. 1*C*). These data suggest that while p85α plays a role in the transition from DN3 to DP upon pre-TCR stimulation, it is not essential because this transition still occurs, albeit less efficiently, in p85α$^{-/-}$ cells.

Lack of p85α has little effect on differentiation of DP into CD4/CD8SP thymocytes

Analysis of p85α$^{-/-}$ mice has previously demonstrated that p85α$^{-/-}$ and p85α$^{+/-}$ mice show little difference in the composition of DN, DP and SP thymocytes (8). The apparent lack of difference may be due to some compensatory mechanisms. Even if the PI3K pathway is involved in the TCR signals for positive and negative selection and the lack of p85α affects the signal strength, thymocytes expressing TCRs of different affinities would have substituted wild-type populations. To examine the role of p85α in positive and negative selection processes without such compensatory effects, we analyzed thymic selection using TCR-tg mice on a p85α$^{-/-}$Rag-2$^{-/-}$ background in which no endogenous TCR can be expressed. DO11.10 mice express an H-2^{d}-restricted TCR specific for an $OVA_{323-339}$ peptide. Thymocytes of p85α$^{-/-}$DO11.10/Rag-2$^{-/-}$ mice develop into CD4 SP cells to a level comparable to p85α$^{+/-}$DO11.10/Rag-2$^{-/-}$ mice (Fig. 2, *A* and *B*, and Table I). Similarly, CD4 SP cell development was unaffected in the absence of p85α in TCR-tg mice expressing another MHC class II-restricted TCR, Cyt5CC7 (Fig. 2*A* and Table I). In addition, CD8 SP cell development appeared normal in the absence of p85α in P14 and OT-I-tg mice expressing MHC class I-restricted TCRs (Fig. 2*A*, Table I and data not shown). These results show that positive selection is unaffected by the lack of p85α. We next investigated the role of p85α in negative selection by in vivo administration of the antigenic peptide, $OVA_{323-339}$, which deletes DP cells in DO11.10 TCR-tg mice (25). As shown in Fig. 2*A* and Table I, no significant difference in the deletion of DP cells was observed between p85α$^{+/-}$ and p85α$^{-/-}$DO11.10/Rag-2$^{-/-}$mice. Furthermore, analysis of TCR Vβ repertoire in thymocyte and splenocyte subpopulations revealed that p85α$^{-/-}$ mice on a BALB/c background had, if any, only slight effect on endogenous superantigen mediated deletion as demonstrated by the deletion of cells expressing Vβ3 and Vβ12 (Fig. 2*C* and data not shown). These results indicate that negative selection is little affected in the absence of p85α as well.

Interestingly, statistics compiled from thymocyte populations showed significant reductions of total as well as DP cell numbers in p85α$^{-/-}$DO11.10/Rag-2$^{-/-}$ mice compared with p85α$^{+/-}$DO11.10/Rag-2$^{-/-}$ mice (Fig. 2*B*). In contrast, DN cell numbers were similar between p85α$^{+/-}$ and p85α$^{-/-}$DO11.10/Rag-2$^{-/-}$ mice. Although DP cell numbers were decreased in p85α$^{-/-}$DO11.10/Rag-2$^{-/-}$ mice, annexin V-positive DP cells were not enriched compared with control mice (data not shown), indicating that cell death is not particularly enhanced in the absence of p85α. Thus, the reduction of DP cell numbers is unlikely due to increased apoptosis mediated by negative selection or death by neglect, but rather reflects the delayed transition from the DN3 to DP stage as shown in p85α$^{-/-}$Rag-2$^{-/-}$ mice (Fig. 1). Although CD4 SP cell numbers appeared slightly lower in p85α$^{-/-}$DO11.10/Rag-2$^{-/-}$ mice than p85α$^{+/-}$DO11.10/Rag-2$^{-/-}$ mice, it may reflect decreased numbers of p85α$^{-/-}$DO11.10/Rag-2$^{-/-}$ DP cell but not the defects during positive selection.

p110δ is decreased in p85α$^{-/-}$ DN cells

The *Pik3r1* gene encodes three alternatively spliced products, p85α, p55α and p50α (4–7). Because our targeting strategy only deletes p85α, potentially leaving the p55α and p50α isoforms intact, the expression levels of these alternative isoforms in p85α$^{-/-}$ cells may differ from those in wild-type cells. As shown previously (10), the expression of p110δ is greatly decreased in p85α$^{-/-}$ B cells (Fig. 3*A*), likely contributing to the observed B cell phenotypes in p85α$^{-/-}$ mice (8, 10). In contrast, DP thymocytes in p85α$^{-/-}$ mice express higher levels of p55α/p50α than those in wild-type mice and expression levels of p110δ were comparable between p85α$^{-/-}$ and p85α$^{+/-}$ mice (Fig. 3*A*).

Since we observed the effect of p85α deficiency only at the DN to DP transition, it was of interest to examine expression levels of PI3K subunits during thymocyte development and to correlate this

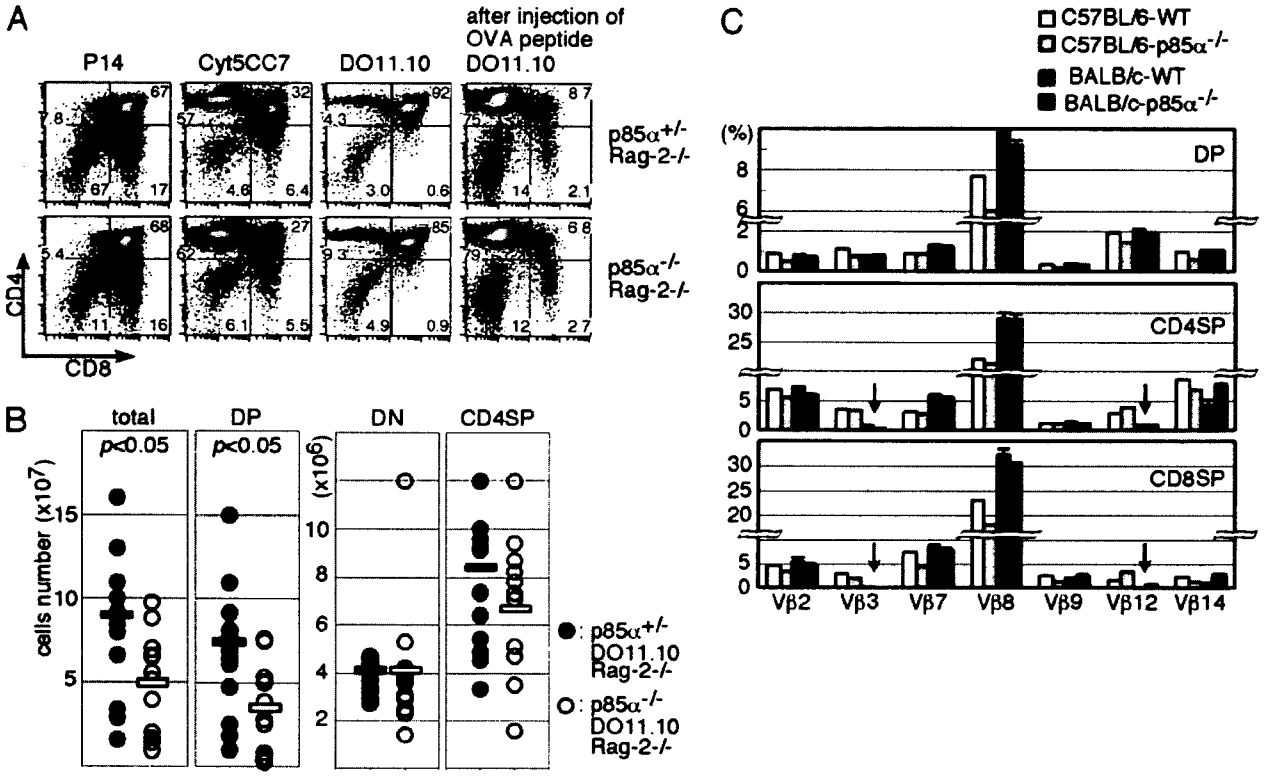

FIGURE 2. The effect of p85α deficiency on thymic selection in TCR-tg mice on a Rag-2$^{-/-}$ background. *A*, CD8/CD4 surface phenotypes were examined in P14, Cyt5CC7, and DO11.10-tg mice on p85α$^{-/-}$Rag-2$^{-/-}$ and p85α$^{+/-}$Rag-2$^{-/-}$ backgrounds. In addition, p85α$^{-/-}$DO11.10/Rag-2$^{-/-}$ and control mice were injected with $OVA_{323-339}$ peptide i.v. 72 h before analysis. Numbers are percentages of each population. *A* is representative of two independent experiments. *B*, Analysis of total thymocyte numbers and absolute numbers of DP, DN, and CD4SP cells in p85α$^{-/-}$DO11.10/Rag-2$^{-/-}$ mice (n = 14) and control mice (n = 15). Each circle represents a single mouse and open and bold bars indicate the mean values of p85α$^{-/-}$DO11.10/Rag-2$^{-/-}$ and control mice, respectively. Total and DP cell numbers in p85α$^{-/-}$DO11.10/Rag-2$^{-/-}$ mice are significantly ($p < 0.05$) lower than those in control mice. *C*, The percentages of CD8SP, CD4SP, and DP thymocytes expressing Vβ2, 3, 4, 7, 8, 9, 12, and 14 were examined in p85α$^{+/+}$ and p85α$^{-/-}$ mice on C57BL/6 and BALB/c backgrounds. Please note that CD8SP and CD4SP cell populations expressing TCR Vβ3 and Vβ12 (indicated by arrows) were efficiently eliminated in both p85α$^{-/-}$ and p85α$^{-/+}$ mice on a BALB/c background.

with thymocyte phenotype. As shown in Fig. 3*B*, expression levels of the p110δ catalytic subunit, the major catalytic subunit expressed in lymphocytes, were significantly lower in thymocytes of p85α$^{-/-}$Rag-2$^{-/-}$ mice than p85α$^{+/-}$Rag-2$^{-/-}$ mice, which are mostly at the DN3 stage. Normalized by the amounts of ERK2, we assessed the reduction of p110δ in p85α$^{-/-}$Rag-2$^{-/-}$ mice to 27 ± 16% (mean ± SD, n = 3) of p85α$^{+/-}$Rag-2$^{-/-}$ mice. The reduced expression level of p110δ is likely due to the reduction of regulatory subunits including p85α, because association
with regulatory subunits stabilizes the catalytic subunits (4–7). Interestingly, the expression level of p50α was increased after anti-CD3ε mAb injection in p85α$^{-/-}$Rag-2$^{-/-}$ mice, and concomitantly the expression level of p110δ in p85α$^{-/-}$Rag-2$^{-/-}$ mice increased to a level similar to that of p85α$^{+/-}$Rag-2$^{-/-}$ mice (Fig. 3*B*).

Table I. *Cell numbers of total, DP, DN, and CD4 or CD8SP thymocyte in TCR-tg mice*[a]

Mice	Total (×10^7 cells)	DP (×10^7 cells)	DN (×10^6 cells)	SP (×10^6 cells)
P14/Rag-2$^{-/-}$				
p85α$^{+/-}$	8.0 ± 1.0	5.4 ± 0.8	4.8 ± 0.6	6.6 ± 1.6
p85α$^{-/-}$	8.6 ± 2.2	6.5 ± 2.1	5.1 ± 0.7	5.1 ± 0.4
Cyt5CC7/Rag-2$^{-/-}$				
p85α$^{+/-}$	7.0 ± 2.8	1.6 ± 0.9	4.1 ± 1.0	39 ± 17
p85α$^{-/-}$	7.3 ± 1.9	1.5 ± 0.5	4.0 ± 1.3	40 ± 16
DO11.10/Rag-2$^{-/-}$				
p85α$^{+/-}$	9.0 ± 1.4	7.4 ± 1.3	4.1 ± 0.3	8.4 ± 1.2
p85α$^{-/-}$	5.0 ± 0.9[b]	3.5 ± 0.8[b]	4.1 ± 0.8	6.7 ± 0.8
DO11.10/Rag-2$^{-/-}$ (After OVA injection)				
p85α$^{+/-}$	4.9 ± 1.2	1.70 ± 0.64		
p85α$^{-/-}$	2.3 ± 0.2	0.20 ± 0.06		

[a] CD8/CD4 surface phenotypes of each mouse are shown in Fig. 2*A*. Data shown are means ± SEM from more than two independent experiments.

[b] Total and DP cell numbers in p85α$^{-/-}$DO11.10/Rag-2$^{-/-}$ mice are significantly ($p < 0.05$) lower than those in control mice.

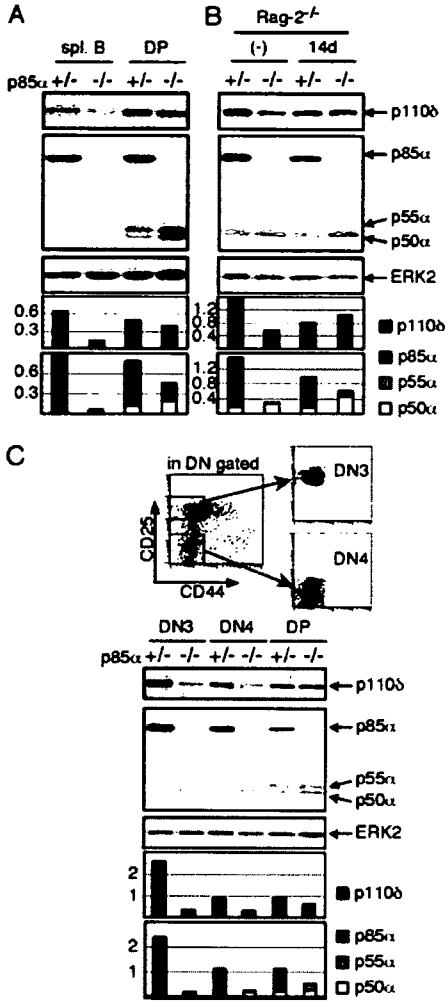

FIGURE 3. Evaluation of expression levels of PI3K subunits by Western blot analysis. *A*, Expression levels of p85α/p55α/p50α and p110δ were examined in splenic B cells and DP thymocytes from $p85\alpha^{-/-}$ and $p85\alpha^{+/-}$ mice. *B*, Expression levels of p85α/p55α/p50α and p110δ were examined in thymocytes from $p85\alpha^{-/-}$Rag-$2^{-/-}$ and $p85\alpha^{+/-}$Rag-$2^{-/-}$ mice without anti-CD3ε mAb injection (−) and at 14 days after injection. *C*, DN3 and DN4 cells were sorted according to CD44/CD25 surface profiles from $CD8^-CD4^-CD3\varepsilon^-$ thymocytes of $p85\alpha^{-/-}$ or $p85\alpha^{+/-}$ mice (*upper panels*). DP cells were also sorted from $p85\alpha^{-/-}$ or $p85\alpha^{+/-}$ mice. Purity was >99% in each population. Expression levels of p85α/p55α/p50α and p110δ were examined in DN3, DN4, and DP cells from $p85\alpha^{-/-}$ mice and $p85\alpha^{+/-}$ mice (*lower panel*). Estimated protein levels of p85α/p55α/p50α and p110δ, which were normalized by the amounts of ERK2, are indicated below.

We next sorted DN3, DN4, and DP cells and examined them for expression levels of PI3K subunits (Fig. 3*C*). The expression level of p110δ in DN3 cells was higher than that in DN4 or DP cells as normalized by ERK2 levels (the ratio of p110δ to ERK2 was 2.4 ± 0.18, 0.94 ± 0.17, and 0.86 ± 0.22 in DN3, DN4 and DP cells, respectively, mean ± SD, $n = 3$). In addition, when we compared expression levels of p110δ between $p85\alpha^{-/-}$ and $p85\alpha^{+/-}$ cells, it was clear that the amount of p110δ was significantly lower in $p85\alpha^{-/-}$ DN3 and DN4 cells than those of heterozygotes. In contrast, p110δ levels in DP cells were not significantly affected by the lack of p85α (Fig. 3*C*). We noted that expression levels of p55α were increased in DP cells and DP cells express higher amounts of p55α/p50α subunits than DN3 and DN4 cells (Fig. 3, *A* and *C*). Such enhanced expression of p55α/p50α likely contributes to the stabilization of p110δ in DP cells, leading to the increase in expression levels of p110δ in the DP cells as compared with DN3 and DN4 $p85\alpha^{-/-}$ cells.

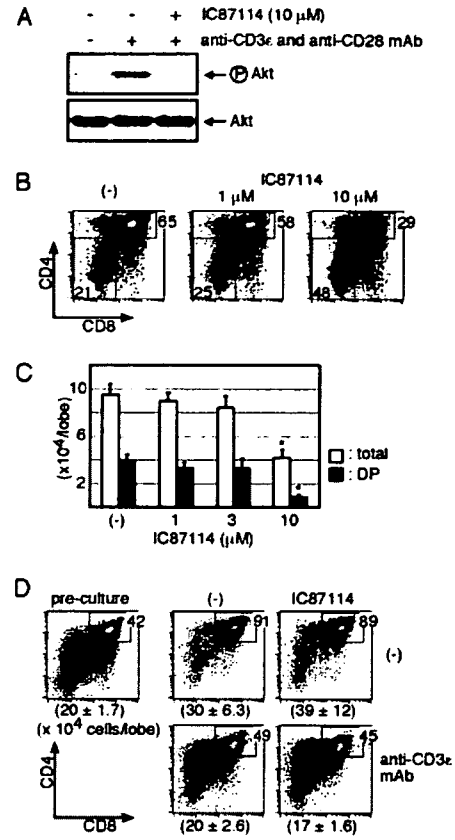

FIGURE 4. The effect of IC87114 on early thymocyte development in E14.5 FTOC. *A*, Splenic T cells derived from wild-type mice were stimulated with anti-CD3ε and anti-CD28 mAb (10 μg/ml each) for 5 min in the presence or absence of 10 μM IC87114. Activation of Akt was evaluated by Western blotting with anti-phospho-Akt mAb. *B*, CD8/CD4 surface phenotypes were examined in E14.5 FTOC cultured with the indicated concentrations of IC87114 for 5 days. *C*, Cell numbers per lobe of total and DP cells are shown as mean ± SEM of four independent experiments. Total and DP cell numbers in fetal thymi cultured with 10 μM IC87114 are significantly lower than untreated lobes (*, $p < 0.01$). *D*, CD8/CD4 surface phenotypes were examined in E17.5 FTOC cultured without (−) or with 10 μg/ml anti-CD3ε mAb in the presence or absence (−) of 10 μM IC87114 for 24 h. Numbers are percentages of DP population. Total cell numbers per lobe were also examined and indicated below (mean ± SEM, $n = 4$).

p110δ is involved in the transition of DN to DP cells in fetal thymocytes

Because our data raise the possibility that p110δ regulates the transition of DN to DP thymocyte upon pre-TCR stimulation, we examined the effect of a selective p110δ inhibitor IC87114 on an early thymocyte development with embryonic day 14.5 (E14.5) FTOC. As has been reported (24), IC87114 blocked Akt phosphorylation, a measure of PI3K activity, in splenic T cells stimulated with anti-CD3ε and anti-CD28 mAb (Fig. 4*A*). Addition of IC87114 in E14.5 FTOC derived from wild-type mice significantly decreased the induction of DP cells in a dose-dependent manner (Fig. 4, *B* and *C*). IC87114 treatment did not induce cell death because cell viability was estimated as 95 ± 5% (mean ± SD) of control culture by 7AAD staining. IC87114 thus blocked pre-TCR induced DN to DP transition without affecting cell viability. In contrast, E17.5 thymocytes, which are at DN4 and DP stages in the

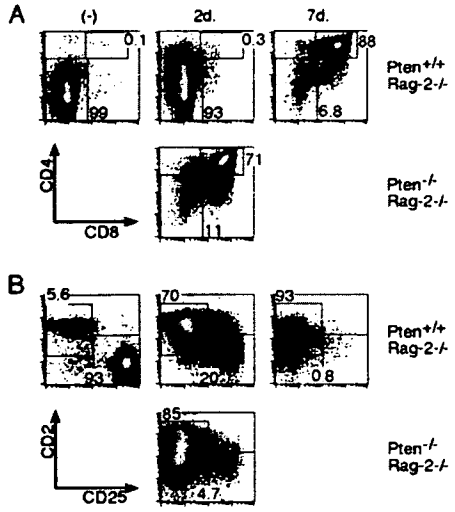

FIGURE 5. DP cell transition is accelerated in Pten$^{-/-}$Rag-2$^{-/-}$ mice compared with Pten$^{+/+}$Rag-2$^{-/-}$ mice upon anti-CD3ε mAb stimulation. *A* and *B*, CD8/CD4 and CD25/CD2 surface phenotypes were examined in Pten$^{-/-}$Rag-2$^{-/-}$ and Pten$^{+/+}$Rag-2$^{-/-}$ mice at the indicated times after injection. Numbers are percentages of DN and DP populations in *A* and CD2^{+}CD25^{-} and CD2^{-}CD25^{+} populations in *B*. Figures are representative of three independent experiments.

beginning of the culture, showed little difference in subsequent SP cell development even in the presence of IC87114 (data not shown). In addition, IC87114 had little effect on DP thymocyte deletion induced by anti-CD3ε mAb in E17.5 FTOC, suggesting that p110δ plays a limited role in negative selection (Fig. 4*D*), which is consistent with the results shown in Fig. 2. These results collectively indicate that p110δ is involved in the pre-TCR signal during DN to DP transition but not in subsequent transition to SP thymocytes in both adult and fetal thymus.

Loss of Pten accelerates transition of DN to DP cells

Generation of PI(3,4)P_2 and PI(3,4,5)P_3 by PI3Ks is reversible and is opposed by a specific lipid phosphatase, termed Pten. It is known that the absence of Pten causes sustained PI3K signaling. To further confirm that lipid products generated by PI3Ks are involved in transition of DN to DP cells, we crossed Pten$^{flox/flox}$ mice, Rag-2$^{-/-}$ mice and Lck-Cre-tg mice to generate Rag2$^{-/-}$ mice with T cell specific deletion of Pten. Lck-Cre/Pten$^{flox/flox}$ mice and Pten$^{flox/flox}$ mice were described here as Pten$^{-/-}$ and Pten$^{+/+}$ mice, respectively. Pten deficiency had no effect on expression levels of p85α and p110δ in thymocytes on a Rag-2$^{-/-}$ background (data not shown). We then injected anti-CD3ε mAb into Pten$^{-/-}$Rag-2$^{-/-}$ and Pten$^{+/+}$Rag-2$^{-/-}$ mice. Without anti-CD3ε mAb stimulation, most Pten$^{-/-}$Rag-2$^{-/-}$ thymocytes remain at the DN3 stage as observed in Rag-2$^{-/-}$ mice. However, two of seven mice spontaneously developed DP cells and such DP cells showed an unusual CD2^{+}CD25^{+} phenotype (data not shown). Mice with such DP cells were also found after anti-CD3ε mAb injection. We thus excluded mice with such unusual CD2^{+}CD25^{+} DP cells from further analyses because those mice would have had such DP cells even before anti-CD3ε mAb injection. CD25 is down-regulated and CD2 up-regulated upon β-selection and CD2^{-}CD25^{+} Rag-2$^{-/-}$ DN3 cells become CD2^{+}CD25^{-} cells immediately after anti-CD3ε mAb stimulation before reaching the DP stage (Ref. 23 and Fig. 5*B*). Two days after anti-CD3ε mAb injection, CD2^{+}CD25^{-} DP cells were observed in Pten$^{-/-}$Rag-2$^{-/-}$ mice while CD2 was induced in most of the cells without transition into DP cells in Pten$^{+/+}$Rag-2$^{-/-}$ mice (Fig. 5). As demonstrated in Fig. 1, these cells became DP cells 7 days after anti-CD3ε mAb injection. Moreover, total thymocyte numbers at 2 days after injection were higher in Pten$^{-/-}$Rag-2$^{-/-}$ mice than Pten$^{+/+}$Rag-2$^{-/-}$ mice ($99 \pm 28 \times 10^6$, $n = 4$ vs $11 \pm 4 \times 10^6$, $n = 5$, respectively). It should be noted that expression profiles of developmental markers such as CD8/CD4 and CD25/CD2 (Fig. 5) as well as thymocyte numbers (data not shown) in Pten$^{-/-}$Rag-2$^{-/-}$ mice at 2 days after anti-CD3ε mAb injection were quite similar to those in Pten$^{+/+}$Rag-2$^{-/-}$ mice at 7 days after injection. These data indicate that the loss of Pten dramatically accelerates transition of DN3 to DP cells and that the lipid products generated by PI3Ks are indeed involved in pre-TCR signals.

Discussion

Initial studies on p85α-deficient mice have shown that development and function of B cells are impaired but those of T cells are grossly normal (8, 9). As demonstrated here, when we focused on the β-selection process using the unique system by injecting anti-CD3ε mAb into Rag-2$^{-/-}$ mice, it was revealed that the lack of p85α delayed transition of DN to DP cells. Previous studies have shown that the proliferation of peripheral T cells is attenuated in mice expressing an inactive form of p110δ or Akt (13, 26), suggesting that the PI3K/Akt pathway modulate TCR signals. If this is also the case in the thymus, positive and negative selection would be affected by the lack of p85α that altered the TCR repertoire selection but total cell numbers after selection may not be different between p85α$^{+/-}$ and p85α$^{-/-}$ mice. Accordingly, the p85α deficiency phenotype may have been hidden in previous studies. Indeed, p85α$^{-/-}$DO11.10/Rag-2$^{-/-}$ mice expressing a defined TCR with no endogenous TCRs showed a decrease in DP cell numbers compared with control mice. Furthermore, a p110δ-selective inhibitor, IC87114, suppressed development of DP cells in E14.5 FTOC after 5 days in culture, indicating that p110δ is involved in the transition of DN to DP cells in fetal thymus as well. Interestingly, p85α deficiency had little effect on DP cell numbers in some TCR-tg mice such as Cyt5CC7, P14, and OT-I on a Rag-2$^{-/-}$ background. These differences could be explained by the fact that the expression level of TCR in each tg mouse varies according to promoter and copy numbers of transgene. In addition, the timing of transgene expression varies in different tg mice. Thus, a higher expression level of TCRβ in DN3 might generate strong signal enough to overcome the attenuation of DN to DP transition caused by lack of p85α. In contrast to the effect of the DN to DP transition, positive and negative selection was unaffected in the absence of p85α. We noted that expression levels of p110δ in p85α$^{-/-}$ DP and SP cells were comparable to those of wild-type counterparts, likely due to increased expression of p55α/p50α. Although the lack of p85α would also affect the expression level of p110α expressed in thymocytes (12), we were not able to examine the amounts of p110α in p85α$^{-/-}$ thymocytes due to lack of an appropriate Ab. However, immunoprecipitation of p110δ from total thymocyte lysates resulted in nearly complete depletion of p85α/p55α/p50α (our unpublished observations), indicating that p110δ is indeed the major catalytic subunit and the contribution of p110α must be marginal, if any. Expression levels of p110δ in wild-type DN3 cells were higher than those in DN4 or DP cells (Fig. 3*C*), suggesting an important role for p110δ in β-selection rather than thymic selection at DP stage. Indeed, when we analyzed E14.5 FTOC for 7 and 9 days or E17.5 FTOC for 5 days, no defect in subsequence development of SP cells was observed in the presence of IC87114 (our unpublished observations). Similarly, a previous

study also reported that the inhibition of p110δ function by IC87114 had little effect in FTOC in 7-day cultures (20).

Our observation is consistent with a report demonstrating that mice with a reduced expression level of PDK1, which functions downstream of PI3Ks, as well as mice with T cell specific deletion of PDK1 show impaired expansion of thymocytes (18). Mice deficient for p110γ, the catalytic subunits of class IB PI3K, have decreased thymocyte numbers compared with wild type (27). Although the substrate specificity of class IB PI3K which consists of a catalytic subunit p110γ and a regulatory subunit p101 is similar to that of class IA PI3K, class IB PI3K is activated by G-protein-coupled receptors including chemokine receptors. Interestingly, it was shown that introduction of a constitutively active mutant of class IA PI3K was able to restore the defect of p110γ$^{-/-}$ mice (28). Rodríguez-Borlado et al. (28) have reported that forced expression of a mutant form of p85α leading to activation of catalytic subunits resulted in acceleration of CD4 SP cell differentiation without affecting CD8 SP cells. In contrast, tg mice established by Barbee and Alberola-Ila (12) that express a portion of p110α subunit that lacks catalytic activity but binds p85α, leading to activation of the endogenous catalytic subunit showed no difference in CD4/CD8 commitment. Our results are consistent with the latter report and there was no difference in differentiation to CD4 SP and CD8 SP cells. However, these tg mice show no difference in DN or DP populations compared with non-tg controls. The reason for such discrepancy is unknown at the moment but difference in TCR repertoire may have compensated for the defects as discussed above, because mice used in previous studies were not on a Rag2$^{-/-}$ background. Interestingly, a recent report has shown that thymocyte numbers are significantly lower in p110γ$^{-/-}$p110δ$^{-/-}$ double knockout mice than individual single-deficient mice, likely due to not only facilitation of apoptosis in DP cells but also defects in β-selection (19, 20). The more severe phenotype of p110γ$^{-/-}$ p110δ$^{-/-}$ mice likely reflects the fact that the PI3K/Akt-signaling pathway via various receptors synergistically regulates thymocyte development.

In contrast to the deficiency of PI3Ks, the absence of Pten activates the PI3K/Akt-signaling pathway. The loss of Pten dramatically accelerated transition of DN to DP thymocytes and cellular expansion. These observations are consistent with our conclusion that the PI3K/Akt-signaling pathway is involved in pre-TCR signals during the DN to DP transition. As discussed above, thymocytes of two of seven Pten$^{-/-}$Rag-2$^{-/-}$ mice spontaneously developed into DP cells at 9 wk of age without anti-CD3ε mAb injection. Such spontaneous development of DP cells was independent of the age (our unpublished observations) and such DP cells showed an abnormal phenotype as they express both CD2 and CD25. The loss of Pten is often associated with tumorigenesis (29) and it is possible that the loss of Pten leads to thymoma generation. In the case of T cell-specific deletion of Pten in mice, the first clinical signs of tumor formation were observed in mice at 6–7 wk and all mice died within 17 wk (22). The observed variability of the thymocyte phenotype of Pten$^{-/-}$ Rag-2$^{-/-}$ mice may be ascribed to the timing of Cre expression. Although the p56^{lck} proximal promoter used here is known to be active in DN1 cells, expression of Pten protein was still detectable in the Pten$^{-/-}$Rag-2$^{-/-}$ thymus (our unpublished observations) where thymocytes are arrested at the DN3 stage. Perhaps the p56^{lck} proximal promoter exhibits altered expression patterns as a transgene. However, anti-CD3ε mAb injection led to complete loss of Pten expression (data not shown), likely due to enhanced activity of p56^{lck} proximal promoter.

The PI3K/Akt-signaling pathway is known to suppress apoptosis, increase cell size due to activation of cellular metabolism, and induce cell cycle progression through expression of cyclins and cytokines (30–32). The levels of BrdU uptake in thymocytes in p85α$^{-/-}$ mice were comparable with those in p85α$^{+/-}$ mice (data not shown), suggesting that proliferation during transition from the DN to DP stages was not affected dramatically by the lack of p85α, although it is possible that slight difference in cell cycle progression leads to difference in DP cell numbers. Additionally, IC87114 suppressed DP cell induction without cell death in E14.5 FTOC, indicating that p110δ is not critical for survival at least at the DN stage. In our preliminary experiments, inhibition of mammalian target of rapamycin, a downstream molecule of the PI3K/Akt-signaling pathway, by rapamycin resulted in blockade of DN to DP transition in E14.5 FTOC (our unpublished observations), raising the possibility that the PI3K/Akt-signaling pathway regulates the β-selection through mammalian target of rapamycin. Future studies with mice where the PI3K/Akt-signaling pathway is perturbed should reveal the molecular mechanisms underlying transition of DN to DP thymocytes.

Acknowledgments

We are grateful to Dr. Akira Suzuki of Akita University and Dr. Tak W. Mak of the Ontario Cancer Institute for providing us with the Pten^{flox} mice. We thank laboratory members for their fruitful discussion and Dr. Linda K. Clayton for critical reading of the manuscript and valuable suggestions. Thank are also due to Drs. C. Sadhu and J. Hayflick of ICOS Corporation for the generous gifts of IC87114.

Disclosures

The authors have no financial conflict of interest.

References

1. Starr, T. K., S. C. Jameson, and K. A. Hogquist. 2003. Positive and negative selection of T cells. *Annu. Rev. Immunol.* 21: 139–176.
2. Michie, A. M., and J. C. Zúñiga-Pflücker. 2002. Regulation of thymocyte differentiation: pre-TCR signals and β-selection. *Semin. Immunol.* 14: 311–323.
3. Gill, J., M. Malin, J. Sutherland, D. Gray, G. Hollander, and R. Boyd. 2003. Thymic generation and regeneration. *Immunol. Rev.* 195: 28–50.
4. Koyasu, S. 2003. The role of PI3K in immune cells. *Nat. Immunol.* 4: 313–319.
5. Okkenhaug, K., and B. Vanhaesebroeck. 2003. PI3K in lymphocyte development, differentiation and activation. *Nat. Rev. Immunol.* 3: 317–330.
6. Deane, J. A., and D. A. Fruman. 2004. Phosphoinositide 3-kinase: diverse roles in immune cell activation. *Annu. Rev. Immunol.* 22: 563–598.
7. Vanhaesebroeck, B., K. Ali, A. Bilancio, B. Geering, and L. C. Foukas. 2005. Signalling by PI3K isoforms: insights from gene-targeted mice. *Trends Biochem. Sci.* 30: 194–204.
8. Suzuki, H., Y. Terauchi, M. Fujiwara, S. Aizawa, Y. Yazaki, T. Kadowaki, and S. Koyasu. 1999. Xid-like immunodeficiency in mice with disruption of the p85α subunit of phosphoinositide 3-kinase. *Science* 283: 390–392.
9. Fruman, D. A., S. B. Snapper, C. M. Yballe, L. Davidson, J. Y. Yu, F. W. Alt, and L. C. Cantley. 1999. Impaired B cell development and proliferation in absence of phosphoinositide 3-kinase p85α. *Science* 283: 393–397.
10. Suzuki, H., S. Matsuda, Y. Terauchi, M. Fujiwara, T. Ohteki, T. Asano, T. W. Behrens, T. Kouro, K. Takatsu, T. Kadowaki, and S. Koyasu. 2003. PI3K and Btk differentially regulate B cell antigen receptor-mediated signal transduction. *Nat. Immunol.* 4: 280–286.
11. Deane, J. A., M. J. Trifilo, C. M. Yballe, S. Choi, T. E. Lane, and D. A. Fruman. 2004. Enhanced T cell proliferation in mice lacking the p85β subunit of phosphoinositide 3-kinase. *J. Immunol.* 172: 6615–6625.
12. Barbee, S. D., and J. Alberola-Ila. 2005. Phosphatidylinositol 3-kinase regulates thymic exit. *J. Immunol.* 174: 1230–1238.
13. Okkenhaug, K., A. Bilancio, G. Farjot, H. Priddle, S. Sancho, E. Peskett, W. Pearce, S. E. Meek, A. Salpekar, M. D. Waterfield, et al. 2002. Impaired B and T cell antigen receptor signaling in p110δ PI 3-kinase mutant mice. *Science* 297: 1031–1034.
14. Clayton, E., G. Bardi, S. E. Bell, D. Chantry, C. P. Downes, A. Gray, L. A. Humphries, D. Rawlings, H. Reynolds, E. Vigorito, and M. Turner. 2002. A crucial role for the p110δ subunit of phosphatidylinositol 3-kinase in B cell development and activation. *J. Exp. Med.* 196: 753–763.
15. Jou, S. T., N. Carpino, Y. Takahashi, R. Piekorz, J. R. Chao, N. Carpino, D. Wang, and J. N. Ihle. 2002. Essential, nonredundant role for the phosphoinositide 3-kinase p110δ in signaling by the B-cell receptor complex. *Mol. Cell Biol.* 22: 8580–8591.
16. Hagenbeek, T. J., M. Naspetti, F. Malergue, F. Garçon, J. A. Nunès, K. B. Cleutjens, J. Trapman, P. Krimpenfort, and H. Spits. 2004. The loss of PTEN allows TCR αβ lineage thymocytes to bypass IL-7 and pre-TCR-mediated signaling. *J. Exp. Med.* 200: 883–894.

17. Ciofani, M., and J. C. Zúñiga-Pflücker. 2005. Notch promotes survival of pre-T cells at the β-selection checkpoint by regulating cellular metabolism. *Nat. Immunol.* 6: 881–888.
18. Hinton, H. J., D. R. Alessi, and D. A. Cantrell. 2004. The serine kinase phosphoinositide-dependent kinase 1 (PDK1) regulates T cell development. *Nat. Immunol.* 5: 539–545.
19. Webb, L. M., E. Vigorito, M. P. Wymann, E. Hirsch, and M. Turner. 2005. Cutting edge: T cell development requires the combined activities of the p110γ and p110δ catalytic isoforms of phosphatidylinositol 3-kinase. *J. Immunol.* 175: 2783–2787.
20. Swat, W., V. Montgrain, T. A. Doggett, J. Douangpanya, K. Puri, W. Vermi, and T. G. Diacovo. 2006. Essential role of PI3Kδ and PI3Kγ in thymocyte survival. *Blood* 107: 2415–2422.
21. Terauchi, Y., Y. Tsuji, S. Satoh, H. Minoura, K. Murakami, A. Okuno, K. Inukai, T. Asano, Y. Kaburagi, K. Ueki, et al. 1999. Increased insulin sensitivity and hypoglycaemia in mice lacking the p85α subunit of phosphoinositide 3-kinase. *Nat. Genet.* 21: 230.
22. Suzuki, A., M. T. Yamaguchi, T. Ohteki, T. Sasaki, T. Kaisho, Y. Kimura, R. Yoshida, A. Wakeham, T. Higuchi, M. Fukumoto, et al. 2001. T cell-specific loss of Pten leads to defects in central and peripheral tolerance. *Immunity* 14: 523–534.
23. Shinkai, Y., and F. W. Alt. 1994. CD3ε-mediated signals rescue the development of $CD4^+CD8^+$ thymocytes in RAG-$2^{-/-}$ mice in the absence of TCR β chain expression. *Int. Immunol.* 6: 995–1001.
24. Sadhu, C., B. Masinovsky, K. Dick, C. G. Sowell, and D. E. Staunton. 2003. Essential role of phosphoinositide 3-kinase δ in neutrophil directional movement. *J. Immunol.* 170: 2647–2654.
25. Murphy, K. M., A. B. Heimberger, and D. Y. Loh. 1990. Induction by antigen of intrathymic apoptosis of $CD4^+CD8^+TCR^{lo}$ thymocytes in vivo. *Science* 250: 1720–1723.
26. Arimura, Y., F. Shiroki, S. Kuwahara, H. Kato, U. Dianzani, T. Uchiyama, and J. Yagi. 2004. Akt is a neutral amplifier for Th cell differentiation. *J. Biol. Chem.* 279: 11408–11416.
27. Sasaki, T., J. Irie-Sasaki, R. G. Jones, A. J. Oliveira-dos-Santos, W. L. Stanford, B. Bolon, A. Wakeham, A. Itie, D. Bouchard, I. Kozieradzki, et al. 2000. Function of PI3Kγ in thymocyte development, T cell activation, and neutrophil migration. *Science* 287: 1040–1046.
28. Rodríguez-Borlado, L., D. F. Barber, C. Hernández, M. A. Rodríguez-Marcos, A. Sánchez, E. Hirsch, M. Wymann, C. Martínez-A, and A. C. Carrera. 2003. Phosphatidylinositol 3-kinase regulates the CD4/CD8 T cell differentiation ratio. *J. Immunol.* 170: 4475–4482.
29. Suzuki, A., J. L. de la Pompa, V. Stambolic, A. J. Elia, T. Sasaki, I. del Barco Barrantes, A. Ho, A. Wakeham, A. Itie, W. Khoo, et al. 1998. High cancer susceptibility and embryonic lethality associated with mutation of the PTEN tumor suppressor gene in mice. *Curr. Biol.* 8: 1169–1178.
30. Ward, S. G., and D. A. Cantrell. 2001. Phosphoinositide 3-kinases in T lymphocyte activation. *Curr. Opin. Immunol.* 13: 332–338.
31. Wymann, M. P., M. Zvelebil, and M. Laffargue. 2003. Phosphoinositide 3-kinase signalling—which way to target? *Trends Pharmacol. Sci.* 24: 366–376.
32. Fruman, D. A. 2004. Phosphoinositide 3-kinase and its targets in B-cell and T-cell signaling. *Curr. Opin. Immunol.* 16: 314–320.

Rac1-mediated Bcl-2 induction is critical in antigen-induced CD4 single-positive differentiation of a $CD4^+CD8^+$ immature thymocyte line

Hiroyo Oda,* Harumi Suzuki,*,[1] Kouhei Sakai,* Seiji Kitahara,* Michael S. Patrick,* Yoshinao Azuma,* Kazuro Sugi,† Toshio Kitamura,‡ Jonathan Kaye,§ and Mutsunori Shirai*

*Department of Microbiology and Immunology, Yamaguchi University School of Medicine, Ube, Japan; †Department of Clinical Research, National Sanyo Hospital, Ube, Japan; ‡Division of Cellular Therapy, Advanced Clinical Research Center, Institute of Medical Science, University of Tokyo, Tokyo, Japan; and §Department of Immunology, The Scripps Research Institute, La Jolla, California, USA

Abstract: Rac1, one of the Rho family small guanosine triphosphatases, has been shown to work as a "molecular switch" in various signal transduction pathways. To assess the function of Rac1 in the differentiation process of CD4 single-positive (CD4-SP) T cells from CD4CD8 double-positive (DP) cells, we used a DP cell line DPK, which can differentiate into CD4-SP cells upon TCR stimulation in vitro. DPK expressing dominant-negative (dn)Rac1 underwent massive apoptosis upon TCR stimulation and resulted in defective differentiation of CD4-SP cells. Conversely, overexpression of dnRac2 did not affect differentiation. TCR-dependent actin polymerization was inhibited, whereas early ERK activation was unaltered in dnRac1-expressing DPK. We found that TCR-dependent induction of Bcl-2 was suppressed greatly in dnRac1-expressing DPK, and this suppression was independent of actin rearrangement. Furthermore, introduction of exogenous Bcl-2 inhibited TCR-dependent induction of apoptosis and restored CD4-SP generation in dnRac1-expressing DPK without restoring TCR-induced actin polymerization. Collectively, these data indicate that Rac1 is critical in differentiation of CD4-SP from the DP cell line by preventing TCR-induced apoptosis via Bcl-2 up-regulation. *J. Leukoc. Biol.* 81: 500–508; 2007.

Key Words: *T lymphocytes · TCRs · apoptosis · thymus*

INTRODUCTION

Rac1 belongs to the Rho family of small guanosine triphosphatases (GTPases), which play critical roles in actin cytoskeletal rearrangement in many cell systems. Among the Rho family GTPases, Rac1 has a broad range of guanine nucleotide exchanging factors (GEFs) and effectors so that the molecule acts as a molecular switch in many aspects of signal transduction pathways. Recent studies using transgenic technology have revealed that Rho family GTPases play crucial roles in thymocyte development and TCR-mediated signal transduction [1]. Ectopic expression of bacterial C3T, which inhibits RhoA, -B, and -C, resulted in decreased numbers of CD4CD8 double-positive (DP) cells in the thymus [2], and transgenic expression of constitutively active RhoA resulted in enhanced positive selection [3]. Constitutively active cdc42 induced massive apoptosis in DP thymocytes [4], suggesting that cdc42 is also involved in T cell development.

Rac consists of three independent genes: Rac1, -2, and -3. Rac1 is expressed ubiquitously, whereas expression of Rac2 is restricted to hematopoietic cells. Rac2-deficient mice showed normal T cell development in the thymus, defective Th1 differentiation caused by decreased IFN-γ production [5], perturbed chemotaxis [6], and defective T cell activation accompanied by decreased ERK activation [7]. Rac2, a component of NADPH oxidase, plays a critical role in reactive oxygen species in phagocytes [8], and recently, Rac1 was shown to play a similar role in human macrophages [9]. Transgenic expression of constitutively active Rac1 (L61) generates DP thymocytes in a $RAG^{-/-}$ background [10] and converts positive selection to negative selection [11], indicating that Rac1 regulates the strength of TCR-mediated signal transduction. Rac1-deficient mice are embryonic-lethal, and neutrophil-specific disruption of Rac1 was reported [12]. Recently, conditional knockout mice for Rac1 in a $Rac2^{-/-}$ background were generated, and differential, critical roles of Rac1 and Rac2 in growth and engraftment of hematopoietic stem cells [13–15] as well as in B cell development [16] were reported. However, the effect of each Rac in T cell development is still unknown. As all three Racs are expressed in T cells, we have studied the role of Rac in T cell development using a dominant-negative (dn) strategy. Using DPK, a DP thymic lymphoma capable of differentiation into CD4 single-positive (SP) cells upon antigenic stimulation in vitro [17], we demonstrate that activation of Rac1 is required

[1] Correspondence at current address: Department of Pathology, International Medical Center of Japan, 1-21-1, Toyama, Shinjuku-ku, Tokyo, 162-8655, Japan. E-mail: hsuzuki@ri.imcj.go.jp

Received October 17, 2005; revised September 20, 2006; accepted October 5, 2006.

doi: 10.1189/jlb.1005585

for generation of CD4-SP T cells. CD4-SP generation was blocked by dnRac1, but not by dnRac2, suggesting that Rac2 is not involved in this differentiation process and also indicating the independent regulation of upstream GEFs for Rac1 and Rac2 in DP cells. We demonstrate further that Rac1 is critical in TCR-mediated Bcl-2 induction, indicating that Rac1 is important in antiapoptotic signal transduction in developing T cells as well as inducing actin cytoskeletal reorganization.

MATERIALS AND METHODS

Construction of retroviral vectors

To construct pMXs-PREP retroviral vector, a *Cla*I fragment of woodchuck post-transcriptional regulatory element (wPRE) sequence [18] and a *Sal*I fragment of puromycin-resistance gene were inserted into the *Cla*I and *Sal*I sites of pMXs-IRES-GFP IRES-GFP [19], respectively. PCR-cloned Rac1N17 cDNA was inserted into pMXs-PREP to produce pMXs-PREP-dnRac1. Retroviral vector pMI.2, which contains the IRES-hCD2 sequence, was a kind gift of Dr. Stephen Levin (University of Washington, Seattle, WA), and PCR-cloned human Bcl-2 cDNA was inserted into the multicloning site of pMI.2 to construct pMI.2-Bcl-2. HR2MU, a retroviral expression vector containing human mutant dnRac2 (D57N), was a kind gift of Dr. David A. Williams (University of Cincinnati Medical Center, OH).

Retroviral transduction

Retrovirus-containing supernatants from vector pMXs-PREP, pMXs-PREP-dnRac1, or HR2MU-transfected 293gp packaging cells [20] with vesicular stomatitis virus-envelope plasmid, were used for infection of DPK cells. Retrovirally transduced cells were selected with 1 μg/ml puromycin and sorted for GFP^{hi} cells without single-cell cloning using a FACSVantage SE (Becton Dickinson, Palo Alto, CA).

Detection of activated Rac1 and Rac2

Activation of Rac1 and Rac2 was evaluated by the standard p21-activated kinase (PAK)-binding domain assay. Briefly, 2×10^7 control- and dnRac1-transduced DPK cells were activated with anti-CD3 and anti-CD28 mAb (5 μg/ml each), followed by goat antihamster polyclonal antibody (20 μg/ml, Jackson ImmunoResearch Lab, West Grove, PA) for 5 min at 37°C. Then, activated Rac protein was precipitated with p21-binding domain (PBD) beads (Upstate Biotechnology, Lake Placid, NY) and was subjected to Western blotting analysis using Rac1-specific mAb (23A8, Upstate Biotechnology) and Rac2-specific antibody (Santa Cruz Biotechnology, CA).

In vitro T cell differentiation culture

DPK differentiation assay was carried out as described elsewhere [17] with some modifications. Briefly, 9×10^5-irradiated DC-I (E^k and ICAM-1-transfected murine fibroblasts) per well in six-well plates were precultured for 24 h, with or without 100 ng/ml staphylococcal enterotoxin A (SEA; Toxin Technology, Sarasota, FL) during the last 2 h of the culture period. Then, 4.5×10^5 DPK cells were added, and the culture was continued for 3 more days at 37°C. The cells were harvested after the indicated culture periods and stained with anti-CD4-PE (GK1.5) and anti-CD8α-biotin (53-6.7) antibodies, followed by Streptavidin-TruRed for flow cytometry. All antibodies and staining reagents were purchased from PharMingen (Palo Alto, CA).

Cell cycle analysis

DPK cells were activated with plate-bound anti-CD3ε mAb (50 μg/ml) for 16 h, fixed with 70% ethanol, and treated with RNaseA (1 mg/ml). Fixed cells were stained with 50 μg/ml propidium iodide (PI) for 3 h at room temperature and analyzed on a FACSCalibur (Becton Dickinson).

Measurement of ERK activation

DPK cells were incubated with 10μg/ml anti-CD3ε antibody at 4°C and cross-linked with antihamster secondary antibody for the indicated time at 37°C. After the indicated period (min) of incubation, cells were lysed and Western blotted with antiphospho-ERK and anti-ERK antibodies (Transduction Lab, Palo Alto, CA).

Staining of polymerized actin

DPK cells were added onto anti-CD3ε plus anti-CD28 mAb-coated (20 μg/ml each) coverslips and cultured for 30 min at 37°C. After removing the supernatant, cells were fixed with 4% paraformaldehyde, followed by permeabilization with 0.1% Triton X-100 and stained with phalloidin-Alexa 594 (Molecular Probes, Eugene, OR) and 4′,6-diamidino-2-phenylindole (DAPI; Molecular Probes).

Flow cytometry

Thymocytes or DPK cells were stained with various combinations of FITC-conjugated anti-CD45.2 (Clone 104), PE-conjugated anti-CD4 (GK1.5), anti-CD5 (53-7.3), biotin-conjugated anti-CD8α (53-6.7), anti-TCR-β (597-H57), Annexin V, anti-CD69 (H1.2F3), anti-CD45.1 (A20), and APC-conjugated anti-CD8α (53-6.7). Stained cells were analyzed by two laser FACSCalibur (Becton Dickinson) for four-color FACS analysis.

Real-time RT-PCR analysis

Total RNA was isolated from cells using the RNeasy kit (Qiagen, Hilden, Germany), and real-time PCR was carried out using the QuantiTect SYBR Green RT-PCR kit (Qiagen) with specific primers for Bcl-2α (5′cctgtggatgactgagtacct3′/5′gagcagggtcttcagagaca3′) and Nor1 (5′aagggcttcttcaagagaac3′/5′tgaaatctgcagtactgacatc3′).

Western blotting

Bcl-2-transduced DPK cells (5×10^5 cells) were lysed and applied to SDS-PAGE. Transferred membranes were Western-blotted with rabbit polyclonal anti-Bcl-2 antisera (PharMingen), and reactive proteins were visualized with ECL chemiluminescent substrates (Cell Signaling Technology, Beverly, MA).

RESULTS

dnRac1 inhibits CD4-SP differentiation

To analyze the detailed function of Rac in TCR-mediated signal transduction during positive selection, we decided to use an in vitro experimental system of CD4-SP differentiation. DPK is a naturally occurring DP thymic lymphoma from AND-TCR transgenic mice [17, 21]. This cell line has been shown to differentiate into CD4-SP cells when cocultured with antigen-loaded APC in vitro [17] and thus, has been used to study signal transduction during positive selection of immature thymocytes [22–24]. A dnRac1 (N17) gene was PCR-cloned into the newly established pMXs-PREP retroviral vector, which contains an IRES-GFP cassette and a mRNA stabilizing element (wPRE) sequence [18] for effective gene expression [25]. Although dnRac1-introduced DPK showed some increase in cell size, expression levels of CD4, CD8, and TCR were indistinguishable from the vector control-infected cells (**Figs. 1a** and **2a**).

As we expected, TCR-induced activation of Rac1 was decreased severely in dnRac1-expressing DPK cells (Fig. 1b). Conversely, TCR stimulation did not induce Rac2 activation in

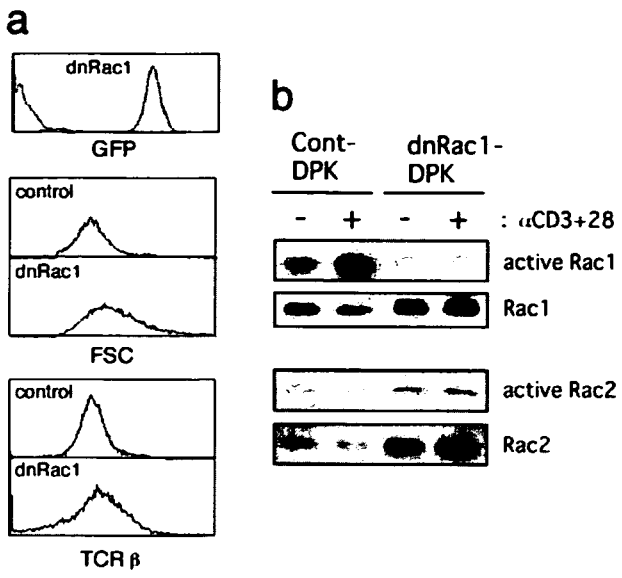

Fig. 1. TCR-induced activation of Rac1 is blocked by introduction of dnRac1. (a) DPK cells infected with pMX-PREP-dnRac1, express dnRac1 protein as well as GFP. Sorted GFP^{hi} cells were analyzed by flow cytometer [forward scatter (FSC)]. (b) TCR stimulation induced Rac1 activation but not Rac2 activation. Control (Cont-DPK; pMXs-PREP) and pMXs-PREP-dnRac1-transduced DPK cells were stimulated with anti-CD3 and -CD28 antibody for 5 min, and active Rac protein was pulled down with PBD beads and subjected to Western blotting analysis using anti-Rac1- and -Rac2-specific antibodies.

vector control-transduced DPK or dnRac1-expressing DPK (Fig. 1b).

As shown in Figure 2a, vector control-transduced DPK cells decreased CD8 expression gradually, and almost 80% of cells differentiated into CD4-SP cells 3 days after antigenic stimulation. In contrast, the generation of CD4-SP cells was abolished almost completely in dnRac1-DPK (Fig. 2a). Addition of Rac1 inhibitor NSC23766 in control DPK also suppressed CD4-SP generation, whereas introduction of dnRac2 (D57N mutation [26]) did not inhibit CD4-SP generation (Fig. 2b).

Lack of CD4-SP generation in dnRac1-expressing DPK could be a result of defective signal transduction or massive apoptosis after antigenic stimulation. We thus examined apoptotic cell death in cultured DPK cells, with or without TCR stimulation. Apoptotic death after 16 h incubation was evaluated by the proportion of cells in the sub-G1 fraction in cell cycle analysis using PI staining (**Fig. 3a**). Control vector expressing DPK showed 21% cell death without stimulation, and this did not increase significantly after TCR stimulation. Conversely, TCR stimulation induced strong cell death in dnRac1-expressing DPK (56%), although it showed augmented cell death without stimulation. At the same time, the number of Annexin V-positive apoptotic cells upon TCR stimulation increased dramatically in dnRac1-DPK compared with control DPK cells (Fig. 3b). Similar results were obtained using the Trypan blue dye exclusion method for determination of cell viability (data not shown). Collectively, expression of dnRac1 in DP thymocytes leads to inhibition of CD4-SP differentiation and augmentation of TCR-induced apoptosis.

Early activation events are intact in dnRac1-expressing DPK

To investigate the function of Rac1 in TCR-dependent signal transduction during positive selection, early activation of ERK was determined. DPK cells were stimulated by anti-CD3ε mAb-coated beads, and activation of ERK was evaluated by phosphorylation of ERK1 and -2 (**Fig. 4a**). The dnRac1 mutant had no effect on ERK activation, indicating that TCR-stimulated activation of ERK was independent of Rac1. We also found that TCR-mediated up-regulation of CD69 and CD5 in dnRac1-DPK cells was indistinguishable from that seen in control DPK cells (Fig. 4b).

Rac-mediated actin polymerization

We next examined TCR-dependent actin polymerization in dnRac1-DPK, as Rac is widely known to play a critical role in cytoskeletal reorganization. After 30 min of TCR stimulation, control DPK cells showed accumulation of polymerized actin and induction of vigorous membrane ruffling, as detected by phalloidin staining, whereas TCR-dependent actin polymerization was abrogated in dnRac1-DPK (**Fig. 5a**). A requirement for actin reorganization during thymocyte development has not been determined directly. Thus, we examined the effect of an inhibitor of actin polymerization on differentiation of DPK cells. Latrunculin A, an inhibitor of actin polymerization [27], blocked antigen-induced CD4-SP cell generation completely in the DPK in vitro differentiation system (Fig. 5b).

Suppression of TCR-mediated induction of Bcl-2

The massive apoptosis in stimulated dnRac1-DPK cells could be a result of an increase in death effectors or a decrease in expression of antiapoptotic proteins, as TCR ligation on DP thymocytes induces death effectors such as Nur77 and Nor1 [28], as well as antiapoptotic molecules such as Bcl-2 and Bcl-xL [29]. To this end, we examined TCR-dependent induction of these molecules in the DPK system. By real-time RT-PCR analysis, a two- to three-fold increase of Bcl-2 mRNA was observed in control DPK cells upon TCR stimulation, whereas stimulation-dependent induction of Bcl-2 was not seen in dnRac1-DPK cells (**Fig. 6a**). Furthermore, induction of bcl-2 was independent of actin polymerization, as Latrunculin A treatment of DPK cells did not inhibit TCR-dependent bcl-2 induction (Fig. 6a). In contrast, TCR-dependent induction of Nor1 in dnRac1-DPK was comparable with that of control cells (Fig. 6b). These data strongly suggest that increased susceptibility to TCR-induced apoptosis in dnRac1-DPK cells is a result of failed induction of antiapoptotic molecule Bcl-2 and not a result of increased induction of death effector molecules.

Restoration of CD4-SP generation by Bcl-2

If the defective positive selection observed in dnRac1-DPK is mainly a result of massive apoptosis caused by insufficient induction of Bcl-2, overexpression of Bcl-2 in dnRac1-DPK should restore positive selection. To this end, we introduced Bcl-2 cDNA retrovirally into dnRac1-DPK cells (**Fig. 7**). Introduction of Bcl-2 enhanced the stimulation-dependent generation of CD4-SP (Fig. 7a), but it is more important that

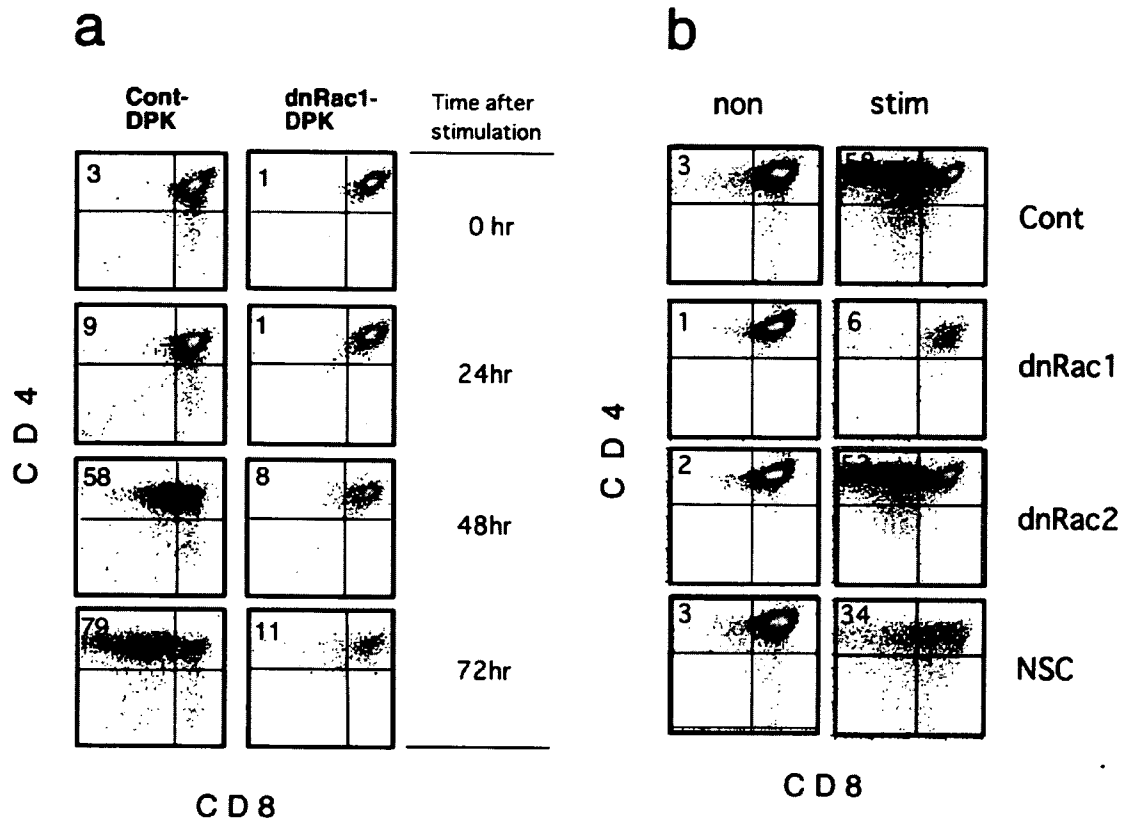

Fig. 2. TCR-induced generation of CD4-SP in vitro is inhibited by dnRac1 but not dnRac2. (a) Vector-only (Cont-DPK) and pMXs-PREP-dnRac1-transduced DPK cells were cocultured with DC-1 and 100 ng/ml SEA. After the indicated culture periods, cells were harvested, and expression levels of CD4 and CD8 were analyzed by flow cytometry. Shown is the phenotype of GFP-positive cells. (b) Cont and dnRac1- and dnRac2-transduced DPK cells were stimulated with or without Rac1 inhibitor NSC23766 (NSC; 20 μg/ml) for 3 days in the same way.

introduction of Bcl-2 restored the generation of CD4-SP in dnRac1-DPK almost completely (Fig. 7, a and c). At the same time, introduction of Bcl-2 attenuated the stimulation-dependent apoptosis observed in dnRac1-DPK (Fig. 7c, lower panel). On the contrary, introduction of Bcl-2 did not restore TCR-induced actin polymerization (Fig. 5a, bottom panels). These results indicate that defective CD4 generation in dnRac1-DPK is mostly a result of the lack of TCR-dependent Bcl-2 up-regulation.

DISCUSSION

Although the effect of constitutively active Rac1 mutant on T cell development has been studied extensively by Cantrell's groups [1, 10, 11], a loss-of-function-type Rac1 mutant study about T cell development has not been reported. Constitutively active Rac1-transgenic mice showed conversion from positive selection to negative selection [11], restoration of the T cell defect in $Vav^{-/-}$ mice, and generation of DP cells in $RAG^{-/-}$ mice [10] suggesting that active Rac1 enhances TCR signal transduction. In the current report, we have shown directly that Rac1 is required for positive selection in an in vitro model system by using dnRac1 and Rac1 inhibitor (Fig. 2). Indistinguishable TCR expression on dnRac1-DPK cells (Fig. 1a) indicates that Rac1 is not involved in assembly and traffic of TCR components to the cell surface.

The inhibitory effect of dnRac1 was stronger than Rac1 inhibitor NSC23766, which inhibits Rac-GEFs Tiam1 and Trio specifically [30] (Fig. 2b). Therefore, these GEFs may not be important in activation of Rac1 in DP cells. As a matter of fact, dedicator of cyto-kinesis 2 (DOCK2)/engulfment and cell motility 1 (ELMO 1) complex is reported to work as a critical Rac1-GEF in TCR-mediated signal transduction [31]. Different from normal DP thymocytes [32], TCR stimulation did not induce Rac2 activation in DPK cells (Fig. 1b). Consistent with the lack of Rac2 activation, overexpression of dnRac2 (D57N mutation [26]) did not inhibit CD4-SP generation (Fig. 2b). It also indicates differential GEF use for Rac1 and Rac2 in TCR-mediated activation in DPK cells.

We found that early ERK activation was not inhibited by the presence of dnRac1 (Fig. 4a). The requirement of ERK activation in positive selection has been well established [33, 34], and PAK1, a major downstream target of Rac1, has been shown to be involved in ERK activation [35, 36]. However, normal ERK activation in dnRac1 DPK indicates that TCR-mediated activation of ERK is independent of Rac1. Thus, the inhibitory effect of dnRac1 on positive selection cannot be attributed simply to inhibition of ERK activation.

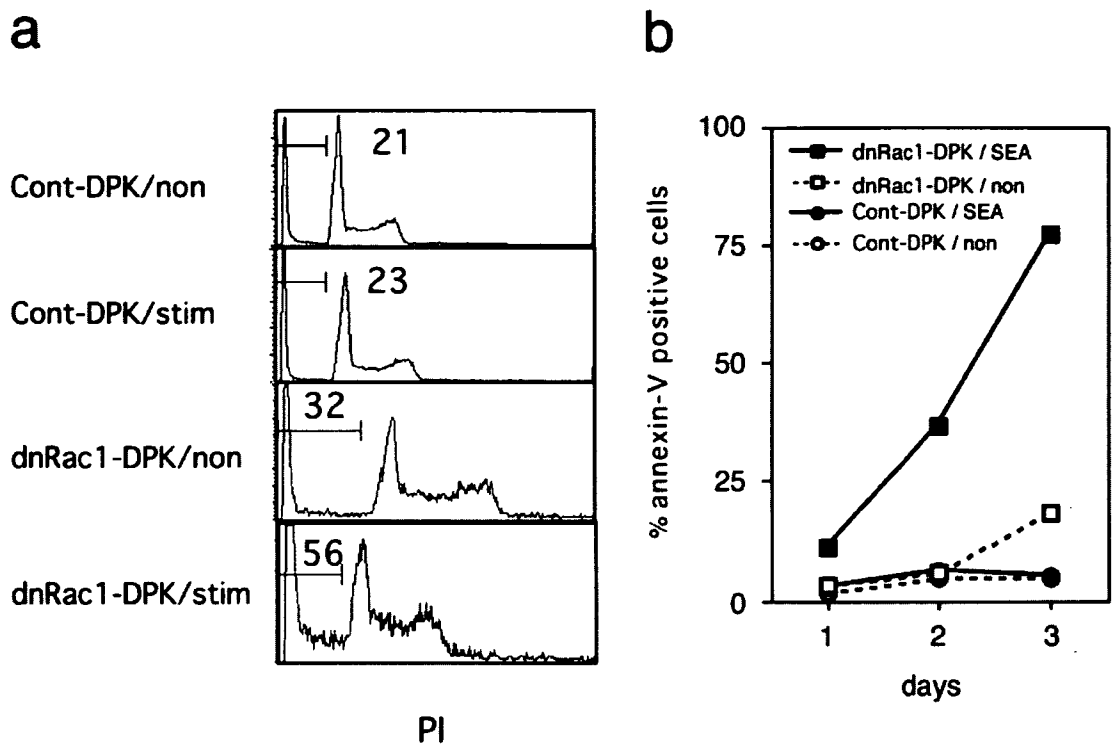

Fig. 3. Expression of dnRac1 increases TCR-induced apoptosis. (a) Stimulation-dependent apoptotic cell death in suspension culture. Vector control or dnRac1-expressing DPK were cultured for 16 h with (stim) or without (non) plate-bound, anti-CD3ε mAb, and cell death was evaluated by DNA content analysis using PI. Numbers show the proportion of cells in the sub-G1 fraction (percent) in cell cycle analysis. (b) GFP-positive dnRac1 or vector control-transduced DPK cells at indicated culture periods were stained with Annexin V, and the proportion of Annexin V-stained cells in each group was plotted.

Rac1 is generally recognized as a key molecule in actin reorganization processes [37]. It is thus not surprising that introduction of dnRac1 prevents TCR-mediated actin polymerization (Fig. 5a). The role of actin cytoskeletal reorganization in T cell development is still not clear, although complete abrogation of positive selection in dn Wiskott-Aldrich syndrome protein transgenic mice [38] and in $Vav^{-/-}$ mice [39] is certainly consistent with a requirement for actin polymerization during positive selection. We demonstrate that actin polymerization is required for positive selection in the DPK system by using an inhibitor of actin polymerization, Latrunculin A (Fig. 5b). However, it is obvious that Rac1-dependent actin polymerization is not required in the differentiation of DPK, as overexpression of Bcl-2 successfully restored CD4-SP differentiation of dnRac1-expressing DPK (Fig. 7) without rescuing the failure of TCR-mediated actin assembly (Fig. 5a). Therefore, a Rac1-independent mechanism of actin polymerization might be required in DPK cell differentiation, or actin polymerization might be critical for antigen presentation in DC-I cells in this experimental system. Recently, TCR-mediated Rac activation and immunological synapse formation have been shown to be dependent on DOCK2 [32]. Impaired positive selection observed in DOCK2-deficient mice [32] is consistent with our finding that Rac1 is critical in positive selection. Rac1 is also reported to be involved in integrin-mediated cell adhesion in thymocytes [40], which is dependent on RhoA [41]. Therefore, it would be interesting to investigate the activity of the integrin in dnRac1-expressing DPK cells.

In the present study, we observed increased TCR-mediated apoptosis in dnRac1-expressing DPK cells (Fig. 3b). Introduction of dnRac1 also affected spontaneous cell death, as we observed increased cell death in dnRac1-expressing DPK, even without stimulation (Fig. 3b). However, this slight increase of spontaneous cell death could not explain the complete loss of stimulation-dependent CD4-SP generation observed in Figure 2b. We therefore don't think that the increase in spontaneous cell death is the major cause of defective CD4-SP generation. At the same time, dnRac1-DPK did not show increased susceptibility to steroid-induced cell death (data not shown). In Jurkat cells, expression of dnRac1 (Rac1-N17) has been shown to protect the cell from Fas-mediated apoptosis [42]. The balance between TCR-mediated induction of proapoptotic and antiapoptotic mediators is a key discriminating factor in positive and negative selection. TCR stimulation of DP thymocytes induces orphan transcription factors Nur77 and Nor1 [28], which play major roles in negative selection [43, 44] by inducing Bim [45, 46] and Fas ligand [47] expression. Induction of the *Nur77* gene is controlled positively by myocyte enhancer factor 2 (MEF2) and negatively by Cabin1 [48] and histone deacetylase 7 [49] via histone deacetylation. TCR signaling releases these repressors from MEF2 to activate *Nur77* transcription. We observed no effect of dnRac1 on induction of these proapoptotic mediators in the DPK system (Fig. 6b). In fact, TCR-mediated Nur77 induction was even lower in dnRac1-DPK compared with control cells (data not shown). These results indicate clearly that increased apoptosis

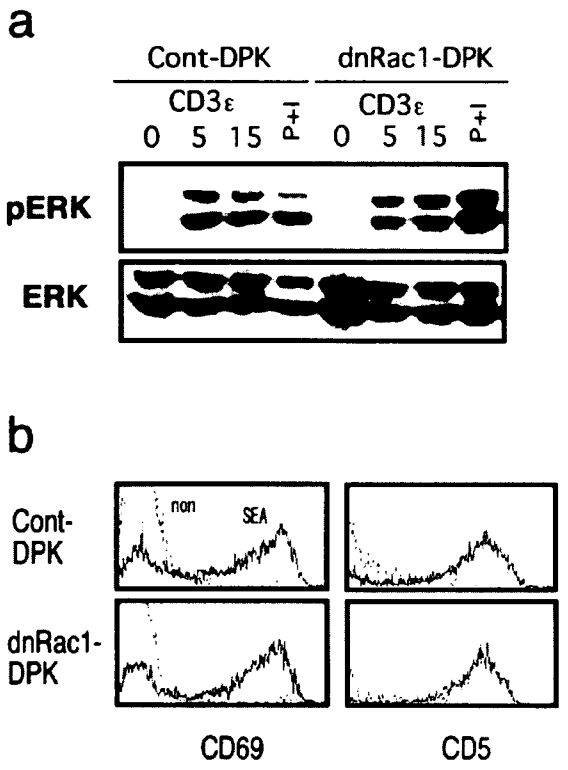

Fig. 4. dnRac1 does not inhibit TCR-dependent, early MAPK activation. (a) DPK cells were activated by anti-CD3ε antibody. After the indicated time (min), cell lysates were prepared and analyzed by Western blotting with antiphospho-ERK (pERK) or anti-ERK antibodies as indicated. P+I, 10 ng/ml PMA and 1 μg/ml A23187. (b) Expression of CD5 and CD69 on dnRac1-DPK cells was analyzed by FACS analysis after 16 h culture with APC in the absence (dotted line) or presence (solid line) of SEA.

in activated dnRac1-DPK cells is not a result of increased expression of proapoptotic mediators.

In contrast, expression of dnRac1 did affect expression of the antiapoptotic mediator Bcl-2 (Fig. 6a). Involvement of Rac1 in the Bcl-2-mediated survival response could be critical in positive selection of thymocytes. Rac2-deficient mast cells were defective in Akt activation and Bcl-xL expression, resulting in impaired survival [50]. Thus, the involvement of Rac proteins in mediating cell survival may be a more general phenomenon. In DP thymocytes, one of the antiapoptotic signals is the exclusion of Nur77 from the nucleus by Akt-dependent phosphorylation of Nur77 [51, 52]. Although we have not examined the phosphorylation status of Nur77 in dnRac1-DPK cells, we think the involvement of Rac1 in regulation of Nur77 phosphorylation is unlikely. TCR-mediated activation of Akt is dependent on PI-3K, and generation of CD4-SP cells in the DPK in the in vitro differentiation system is resistant to PI-3K inhibitors wortmannin and Ly294002 (unpublished observation).

Although Bcl-2-deficient mice showed unimpaired T cell development [53], Bcl-2 is a major antiapoptotic molecule in thymocytes and has been reported to play important roles in their development and maintenance [54]. Bcl-2 expression increases immediately after positive selection [55], and TCR stimulation induces its transcription in vitro as well [29]. Two promoter regions have been identified in the 5′ regulatory region of the Bcl-2 gene, and NF-κB [56] was shown to bind one of these promoter regions. Other studies showed that the Bcl-2 gene is positively regulated by NFAT4 [57] and NF-κB2 [58]. Thus, Rac1 may be involved in TCR-mediated activation of NF-AT or NF-κB to induce Bcl-2 transcription. Consistent with this idea, Rac1 has been shown to be involved in activation of NFAT4 in FcR-mediated signal transduction in mast cells [59].

TCR-dependent induction of Bcl-2 was not inhibited in the presence of Latrunculin A, an inhibitor for actin polymerization (Fig. 6a). At the same time, Latrunculin A did not inhibit TCR-dependent up-regulation of CD69 and CD5 (data not shown). These data suggest that Rac1 affects actin reorganization and Bcl-2 induction independently in DPK cells.

In the present study, we demonstrated that Rac1, but not Rac2, is required for positive selection of a DP cell line. Using the DPK in vitro positive selection model system, Rac1 was shown to be critical in TCR-mediated actin cytoskeletal reor-

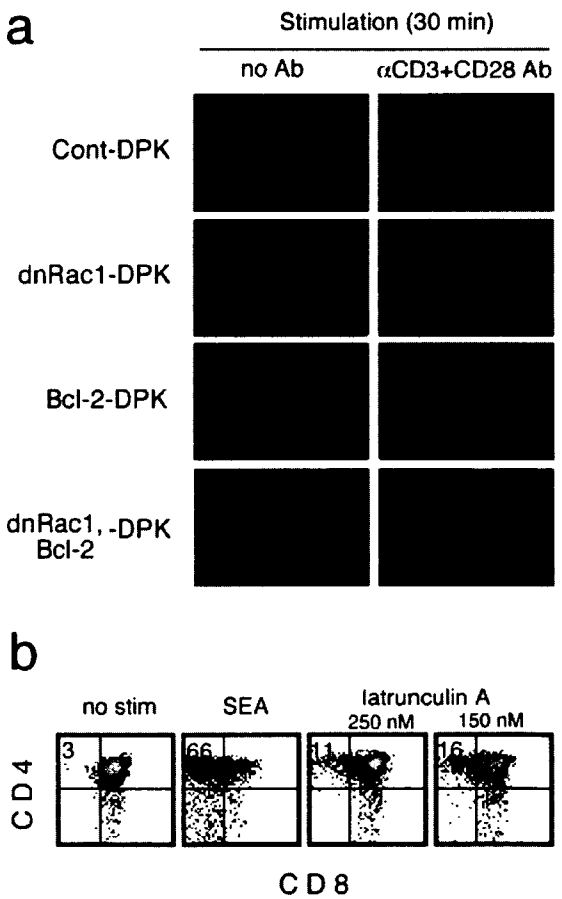

Fig. 5. Rac1 is critical in TCR-dependent actin polymerization. (a) TCR-mediated actin polymerization was inhibited by dnRac1. Vector control or dnRac1-transduced DPK cells were cultured on anti-CD3 and -CD28 mAb-coated coverslips for 30 min and then fixed, permeabilized, and stained with Alexa 594-conjugated phalloidin (red) to detect polymerized actin fibers and DAPI (blue) to visualize nucleus. (b) Generation of CD4-SP cells requires actin polymerization. DPK cells were cocultured with DC-1 and SEA for 3 days in the presence of the indicated concentration of Latrunculin A, an inhibitor of actin polymerization.

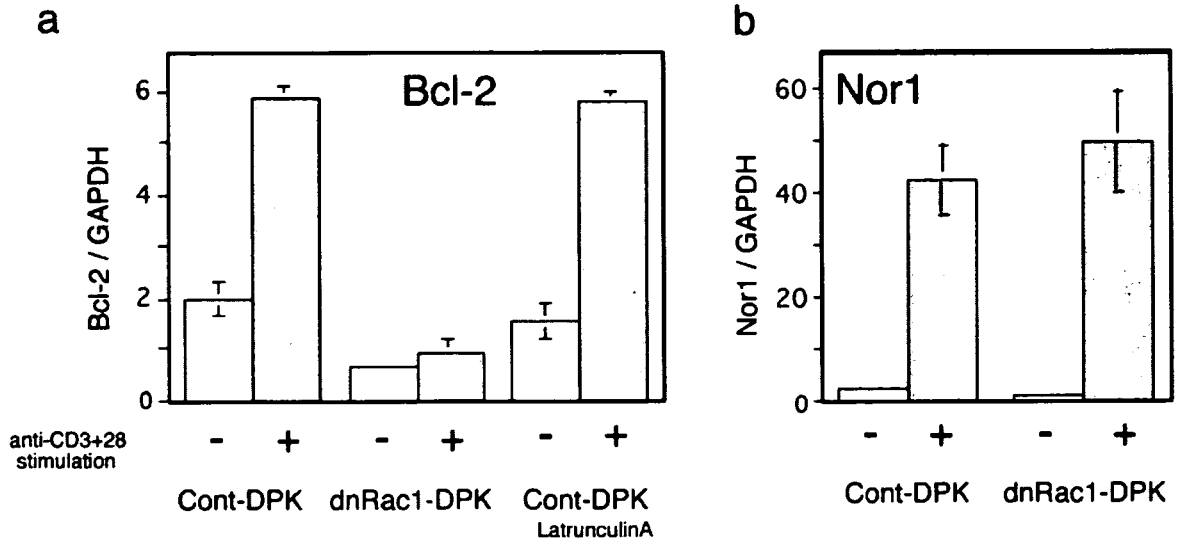

Fig. 6. Effect of dnRac1 on the expression of apoptosis-related genes. Changes in expression of (a) Bcl-2 and (b) Nor1 were determined by quantitative real-time RT-PCR in DPK cells activated with plate-bound anti-CD3 and -CD28 antibodies for 16 h, with or without 150 nM Latrunculin A. Results are presented as a ratio of expression of the indicated gene and the control housekeeping gene GAPDH.

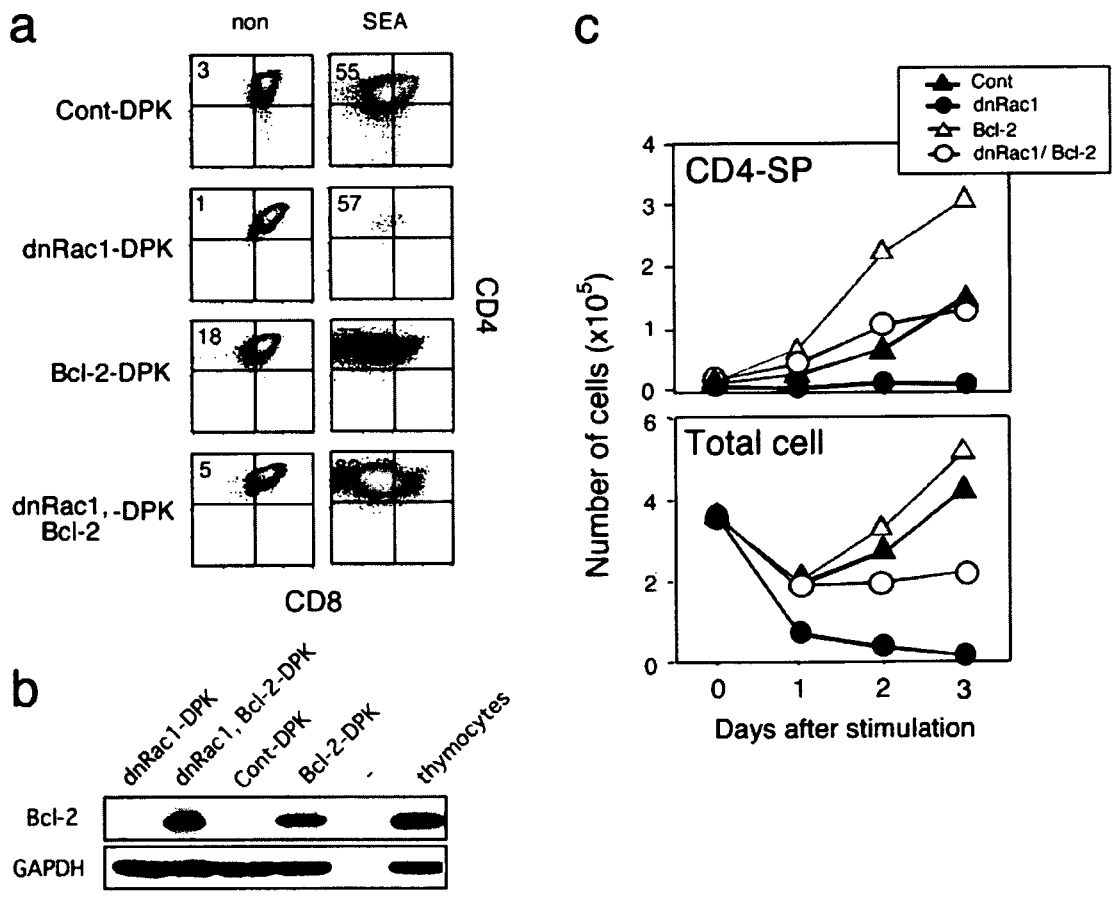

Fig. 7. Overexpression of Bcl-2 rescues CD4-SP generation and attenuates TCR-mediated apoptosis in dnRac1-DPK. (a) DPK cells were transduced with pMXs-PREP vector-only control (Cont-DPK), pMXs-PREP-dnRac1, pMI.2-Bcl-2, or dnRac1 + pMI.2-Bcl-2 and cocultured with DC-1 (non) and 100 ng/ml SEA. After 3 days, cells were harvested and analyzed by flow cytometry. Shown are the CD4 and CD8 profiles of GFP^+ (panels in top two rows and bottom row) and $hCD2^+$ (panels in bottom two rows) cells. (b) Protein expression of Bcl-2 in transduced cells. Cell lysates of each transformant were subjected to SDS-PAGE and Western blotted with anti Bcl-2 antibody. (c) Absolute number of CD4-SP (upper panel) and total cell (lower panel) after indicated culture periods. Number of GFP-positive cells was counted.